Department of
ENERGY TECHNOLOGY E.T.

AALBORG UNIVERSITET
STUDENTERRAPPORT

Analysis Of Two-Phase Flow In A Marine Waste Heat Recovery Exhaust Gas Boiler: Pressure Loss And Heat Transfer Relation

Master's Thesis - Thermal Energy and Process Engineering

Beltrán Galindo Asuar
Michael Skou

AALBORG UNIVERSITY
STUDENT REPORT

Energy, Group TEPE4-1008
School of Engineering and Science
3rd of June, 2014

Title:	Analysis of two-phase flow in a marine waste heat recovery exhaust gas boiler
Semester theme:	Master thesis
Semester:	4^{th} M.Sc.
Project period:	03.02.14 to 03.06.14
ECTS:	60
Supervisor:	Kim Sørensen, Thomas Condra
Project group:	TEPE4-1008

Synopsis:

Boilers are an essential component in the marine WHR field and their performance accounts for a great part of the WHR system efficiency. Although two-phase flow effects are considered in their design it is usually done with very simplistic approximations that come from rules of thumb developed in the industry. This thesis deals with the ellaboration of computer models for the rigurous analysis of the effect two-phase flow has in the essential variables of the boiler operation. Based on a real boiler case both analytical and numerical models are built for the two main two-phase flow study approaches: homogeneous and separated flow. The models are tested for the known working conditions of the boiler on board the ship in order to determine the pressure, quality, temperature and heat flow profiles along the boiler and compare the results with the total pressure loss and heat transfer obtained with the usual design rules of thumb. It is concluded that for a given boiler the analytical homogeneous flow model provides results within a 2% difference of those obtained with the numerical separated flow model for the total heat transfer, but the total pressure loss results differ up to a 60%. The obtained pressure profiles are used to explain the development of the frictional, gravitational and accelerational components of the pressure gradient as evaporation occurs. The most precise of the computer models is also tested under different steam drum pressures, relative positions of the boiler and the drum and mass flows through the system. The characteristic curve of the system is determined and it is concluded that the system is stable and far from reaching the critical heat flux. At the end of the paper some design recommendations to maximize the heat transfer are given: to use lower drum pressures, as a 10% decrease in pressure accounts for 8% more power transfered, and to minimize the distance (pressure loss) between the boiler and the drum, as in the working region an increase of 1 bar in this pressure loss results in 4% heat transfered.

Beltrán Galindo Asuar

Michael Skou

Copies:	5
Pages, total:	92
Appendices:	5
Supplements:	CD

By signing this document, each member of the group confirms that they all participated in the project work and thereby all members are collectively liable for the content of the report.

Nomenclature

Symbol	Description	Unit
A	Area	m^2
C	Coefficient	$-$
c_p	Specific heat capacity	$\frac{J}{kg \cdot K}$
d	Diameter	m
E	Friedel correlation parameter	$-$
E	CISE correlation parameter	$-$
F	Friedel correlation parameter	$-$
f	Friction factor	$-$
Fr	Froude number	$-$
F	Factor	$\frac{m^2}{m}$
G	Mass flux	$\frac{kg}{m^2 \cdot s}$
g	Gravitational acceleration	$\frac{m}{s^2}$
H	Friedel correlation parameter	$-$
h	height	m
h	Specific enthalpy	$\frac{J}{kg}$
ks	Roughness	m
L	Length	m
m	Mass	kg
m	Number	$-$
n	Number	$-$
Nu	Nusselt's number	$-$
Pr	Prandtl's number	$-$
p	Pressure	Pa
q	Heat flux	$\frac{W}{m}$
Q	Heat	W
Re	Reynold's number	$-$
Rr	Relative roughness	$-$
S	Slip ratio	$-$
t	Temperature	°C
T	Temperature	K
U	Heat transfer coefficient	$\frac{W}{m^2 \cdot K}$
u	Actual velocity	$\frac{m}{s}$
V	Superficial velocity	$\frac{m}{s}$
v	Specific volume	$\frac{m^3}{kg}$
W	Work	W
We	Weber number	$-$
w	Width	m

Continued on next page

Continued from previous page

Symbol	Description	
X	Martinelli parameter	$-$
x	Quality	$-$
z	number	$-$
z	distance	m
α	Heat transfer coefficient	$\frac{W}{m^2 \cdot K}$
α	Void fraction	$-$
δ	Thickness	m
η	Dynamic viscosity	$\frac{kg}{m \cdot s}$
λ	Heat conductivity	$\frac{W}{m \cdot K}$
μ	Dynamic viscosity	$\frac{kg}{m \cdot s}$
ϕ	Friction multiplier	$-$
ρ	Density	$\frac{kg}{m^3}$
σ	Surface tension	$\frac{N}{m}$
θ	Angle	$^\circ$
ζ	Resistance	$-$

Prescript

Prescript	Description
d	Differential
Δ	Change

Subscript

a	Acceleration
b	Of the boiler
$Drum$	For the steam drum
ev	Evaporation
exh	For exhaust
ext	External
f	Liquid
f	Friction
fg	Gas liquid difference
fin	For a fin
$fins$	For the fins
g	Vapour
g	Gas
g	Gravitation
go	Gas phase only
h	Heating
h	Homogeneous
i	Inlet
i	Integer

Continued on next page

Continued from previous page

Symbol	Description
in	Internal
l	Saturated liquid
LM	Logarithmic mean
lo	Liquid phase only
o	Outlet
out	External
p	Of a pipe
$pump$	For the pump
qs	Cross-sectional
s	Isentropical
s	Separated
sc	Sub-cooled
s, T	Isentropic
sat	Saturation
$steps$	Number of steps
sub	Subcooled
$tube$	Of the tube
TP	Two-phase
w	Water
ww	Water-ways

Superscript	
$\dot{}$	Flow
$\ddot{}$	Flux
$\bar{}$	Mean/Average

Abbreviations	
WHR	Waste Heat Recovery

Contents

1. Introduction

1.1 Problem statement

Boilers are a key element in waste heat recovery systems installed on board large container ships. Their function is to use excess heat from the engine's exhaust gas to generate steam both to feed turbines for power generation and for its consumption by the steam users on board of the ship.

In the boiler, a stream of water reaches saturation temperature and partially evaporates resulting in a two phase flow of water and steam, but the way this happens, and how it affects the pressure loss along the boiler is rarely studied for their design. In practice, very simple two phase flow models and some time-tested rules of thumb are used to design boilers that satisfy steam demand and size specifications and maximum pressure losses in the exhaust gas and water sides.

This design approach, while being practical and non-time-consuming, can result in over dimensioned equipments and systems in which the effect of different exhaust gas conditions, different heights, relative position of the elements or different pump working curves, is difficult to study and predict.

1.2 Project purpose

The purpose of this project is to build a numerical computer model that considers two-phase flow phenomena in depth, in order to get an accurate pressure loss evaluation and, therefore, an accurate temperature profile along the boiler for a precise heat transfer calculation.

A stable and robust model also allows for parametric searches to study the effect that different variables such as steam demand, position (height) of the boiler in the installation, exhaust gas properties, mass flow or pump work curves have in the performance of the system.

It is also a goal of this project to evaluate whether the simplifications and assumptions being used in boiler design today give precise enough results or not and to assess if a deeper and more complex, and therefore more time consuming and expensive two-phase flow analysis is worth implementing in boiler design strategies, giving comparatively better results and allowing for further optimisation of waste heat recovery systems.

1.3 Methodology

1.3.1 Theory base

Since no empirical data has been used for the elaboration of this paper, all the work presented is based on written material found in books, journals and lecture notes on the subject.

Most of the theory has been extracted from the usual books that professors recommend in two-phase flow university courses, cited in the bibliography. Although this material is somewhat old, its validity has been tested over time: the way these books present the theory, from the definition of two-phase flow to the derivation of the models and their utilization for practical calculations is still up to date and regarded as the standard in this field.

However, a research in scientific articles for more modern approaches to the two-phase flow problem has been made and, whenever these seem to substantially improve the understanding of the physics behind this phenomenon, their utilization has been favored.

1.3.2 Work flow

With the idea of tackling this problem in a way that practical and certain conclussions can be extracted, the method followed has been the same along the whole project: first, the choice of a study case for which enough useful information is available; second, finding a well documented theoretical base which can be transferred into stable computer models; and third, testing these models to ascertain that they produce logical results, with the systematic use of graphics and critical discussion based on the known theory, this is, checking if the obtained results satisfy the physics.

Once the validity of the constructed models is proved, they are tested under different working parameters, obtaining behavioral tendencies of the system which are analyzed and criticised in order to extract practical conclusions that can be translated into real-life recommendations for future design projects.

The following sections of this chapter present the main elements on which this project is based: the existance and working principles of marine waste heat recovery systems and the presence of two-phase flow, and how to study it, in one of the main components of these systems: the boiler.

The chapter ends with a discussion on how this problem is usually dealt with in the boiler design industry.

1.4 Waste Heat Recovery on board large container ships

1.4.1 Waste heat

Waste heat is that contained in the products and subproducts of a process and which has a lower quality, namely lower exergy[1], than the original energy source. In power production plants waste heat is that lost to the environment and which might be used for other applications [1].

In some proccesses, waste heat makes power production byproducts to have a higher temperature than that adequate for their emission or storage.

Waste heat recovery (WHR) systems main purpose is to collect and distribute surplus heat to be used in the same process or others taking part in the plant, such as generating electricity or steam.

Shipping companies install WHR systems on board their container ships to make them more efficient and sustainable, in order to decrease the operation costs, fulfill new emission regulations and laws, and offer a more eco-friendly image to the public.

1.4.2 Waste Heat Recovery Systems

The WHR systems installed on board of large ships usually make use of the Rankine thermodynamic cycle to extract and use the surplus heat contained in the diesel engine's exhaust gas. [2] (Figure 1.1)

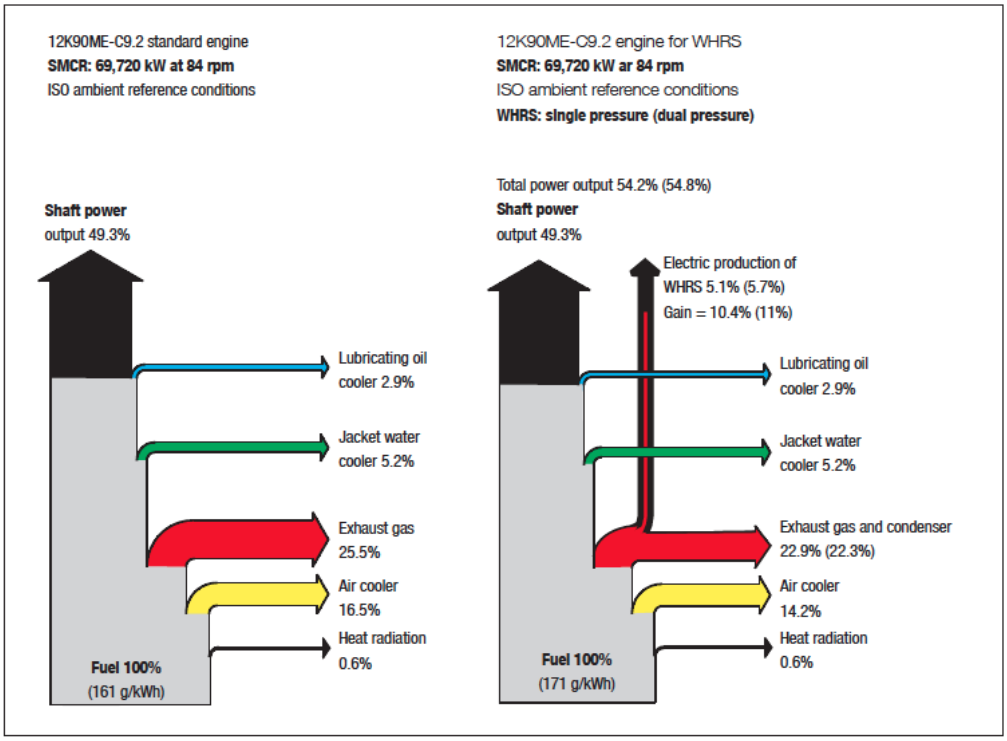

Figure 1.1: Heat distribution on board ships with and without WHR system [3]

[1]Energy that can be transformed into useful work

The heat obtained from the exhaust gas is used to produce steam in an evaporator, which is then sent through a turbine, where it expands, generating mechanical work on its shaft (which is connected to an electric alternator in order to produce electric energy). The low pressure steam that comes out of the turbine is condensed in a condenser, where the heat is sent to a cooling stream. A pump is then in charge of increasing the liquid's pressure to a point where it can be sent to the evaporator again.

Figure 1.2 shows a typical single-pressure marine WHR system[2]. (The preheating section inlet mechanism is not shown).

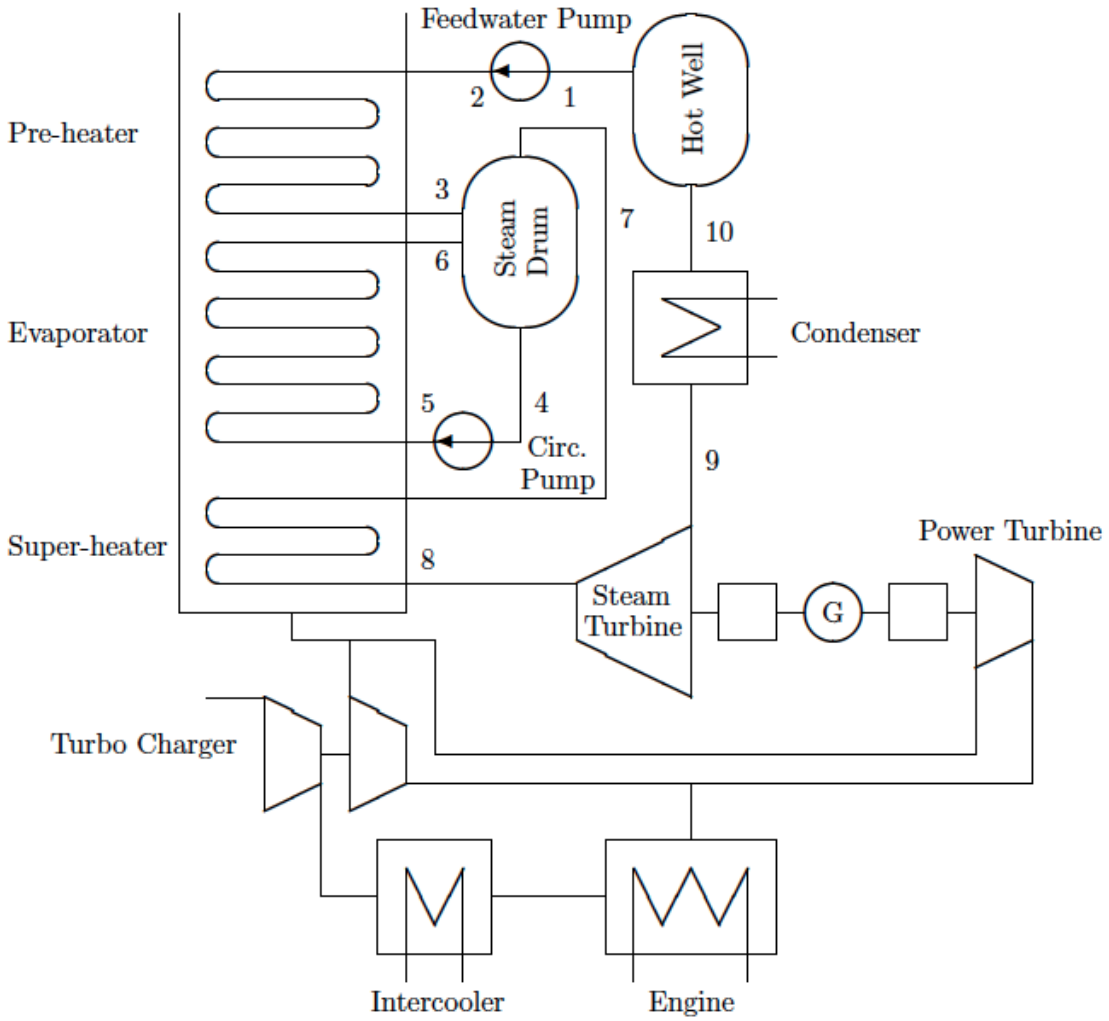

Figure 1.2: Single pressure marine WHR system

[2]See also MAN's WHR catalogue [3]

The steps of the Rankine cycle followed by the system are detailed below:

- 1-2 A pump increases the working fluid's pressure adiabatically.
- 2-3 The temperature of the working fluid is increased in the pre-heater extracting heat from the exhaust gas.
- 3-4 The working fluid is sent to a steam drum.
- 4-5 A circulation pump maintains the flow of the evaporator cycle.
- 5-6 The fluid is partly evaporated in the evaporator which extracts heat from the exhaust gas.
- 6-7 The wet vapour is sent to the steam drum.
- 7-8 Vapour from the steam drum is sent through a super heater which also extracts heat from the exhaust gas.
- 8-9 The superheated vapour is sent through a turbine connected to an electric generator, decreasing both the pressure and temperature of the working fluid.
- 9-10 The working fluid is condensed in a heat exchanger and the excess heat is sent through a cooling system to the sea.
- 10-1 The fluid is sent back to the hot well storage tank.

These processes can also be observed in a T-s diagram (Figure 1.3):

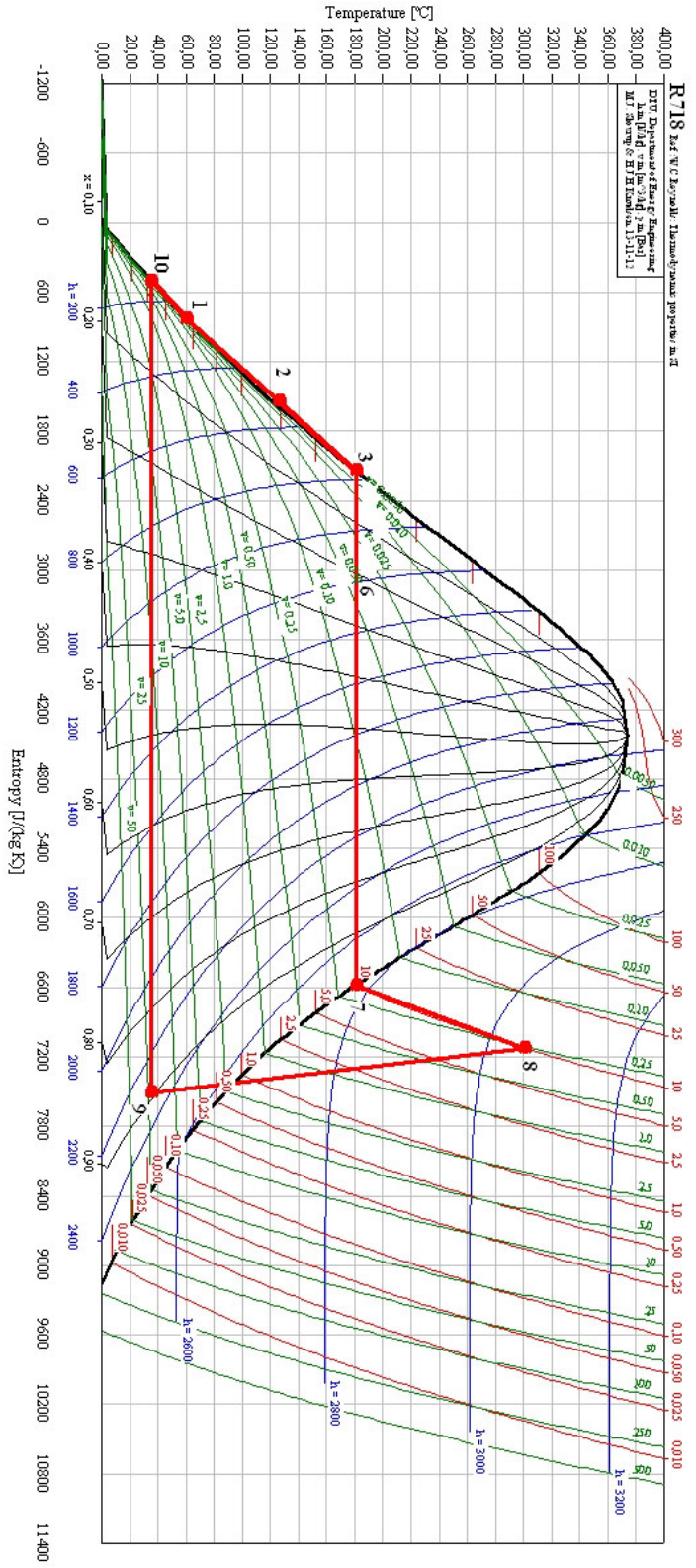

Figure 1.3: T-s diagram of the cycle, for common operation temperatures and pressures

1.5 Two-phase flow

A two-phase flow is that in which two different aggregation states (namely a considerable density difference between phases), of a substance or several, are present at the same time. These can be divided in four different kinds [4]:

- Solid-liquid flow: is when solid particles flow in suspension in a liquid current. Two examples of this can be the presence of sediments in a river or a coal-water slurry.
- Gas-solid flow: solid particles transported by a gas stream. It occurs in the pneumatic transport of grain or in fluidized beds.
- Liquid-liquid flow: is the flow of two inmiscible liquids, which happens, for example, in liquid-liquid extraction processes.
- Gas-liquid flow: a vapour phase flows with a liquid phase. It is present in oil and gas pipelines, areation columns or, in boiling and condensation applications.

This only type of two-phase flow considered in this paper is gas-liquid, as it is the one present in the convective boiling that happens in the evaporators of WHR systems.

In general, the study of a two-phase flow is very complex and requires the establishment of mass, energy and momentum conservation equations and the use of some assumptions and simplifications in order to solve them. Three different approaches have been devised:

- The homogeneous flow model: It is the simplest approach to the problem. The two-phase flow is considered to be a single-phase flow that has average properties obtained from conveniently weighting those of the individual phases. [5]
- The separated flow model: A more complex way of studying the problem, the separated flow model considers the existance of two perfectly segregated phases for which two sets of equations can be written. The interaction between the phases is put into the equations with the aid of empirical correlations. [5]
- The flow pattern models: This is the most sophisticated way of tackling the problem. The way the phases are arranged is determined by comparing their properties to some known flow configurations or patterns of gas and liquid flows in channels. Individual sets of equations exist for each different flow pattern and can be used once the flow has been clasified. [5]

  The patterns of interest for this paper are those determined for horizontal heated pipes, shown in Figure 1.4.

  In order to determine the flow pattern a specific flow has, flow pattern maps based on empirical measurements and correlations like the one in Figure 1.5 have been

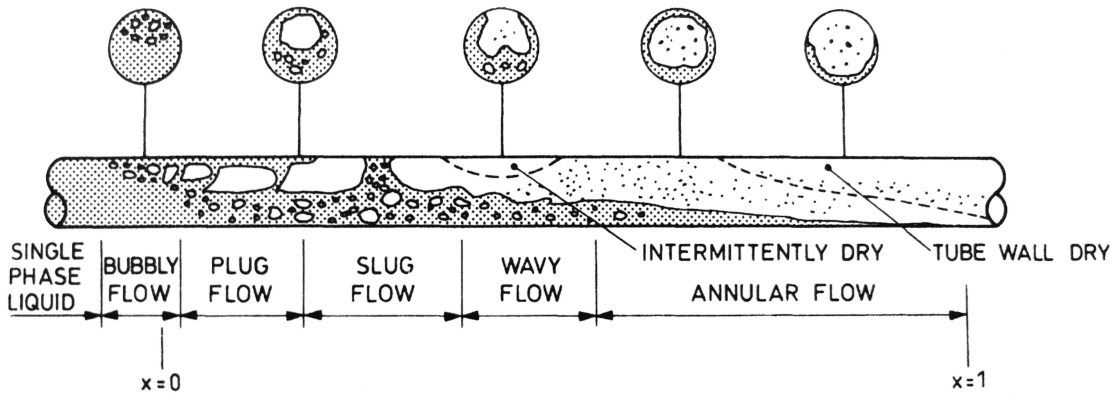

Figure 1.4: Two-phase flow patterns for evaporation in horizontal tubes [5]

developed. These give the flow pattern as a function of two parameters, which depend on the flow conditions.

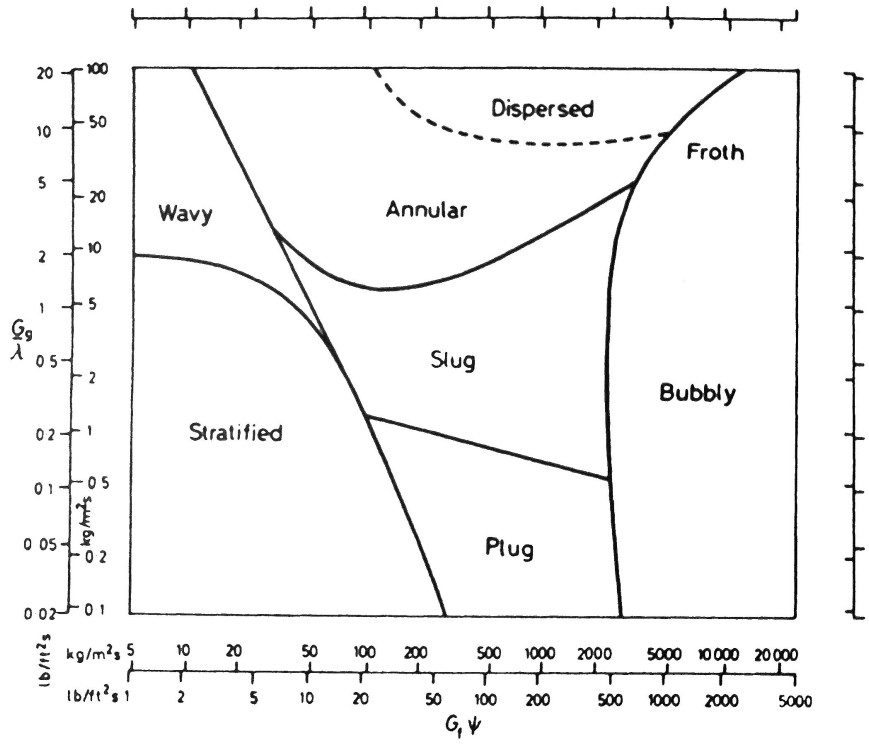

Figure 1.5: Baker flow pattern map for horizontal flow [5]

The basic parameters on which the homogenous and separated flow models are based are described in chapter 3. The use of the flow maps to determine the flow patterns is detailed in section 4.8.

1.6 Pressure loss and boiler design

Due to the pressure loss occasioned by the two-phase flow, the saturation temperature along the boiler can not be considered to be constant because as pressure decreases the temperature at which the two phases coexist decreases as well.

Implementing this notion in the design of the boiler requires complex two-phase flow calculations even, if it is to be done properly, with the construction of numerical models that can determine the local conditions of the flow in every position in the boiler so as to determine the real pressure loss. Once the pressure loss is known, the saturation temperature evolution is known as well, and the amount of heat transfered can be obtained.

It is a common practice in industry, in order to avoid the cost in time and money that developing these numerical models represent, to take the effect of the two-phase flow pressure loss and the sub-cooled section into account by assuming a horizontal saturation temperature line but at an estimated higher saturation pressure. This is, the boiler is still designed as if there was no pressure loss or sub-cooled section (horizontal saturation temperature line) and the effect of the pressure loss is compensated rising this line so the pinch point temperature difference becomes smaller, hence calculating a smaller heat transmission and obtaining the real required heating surface area. [6]

Figure 1.6 illustrates this idea with an example. The exhaust gas temperature is shown in red, the real water temperature profile, including the sub-cooled length and the effect of the pressure loss is shown in blue. Instead of calculating the boiler using a horizontal line at 175 °C, it is raised to 188 °C (dotted line), being this the temperature profile used for the calculations.

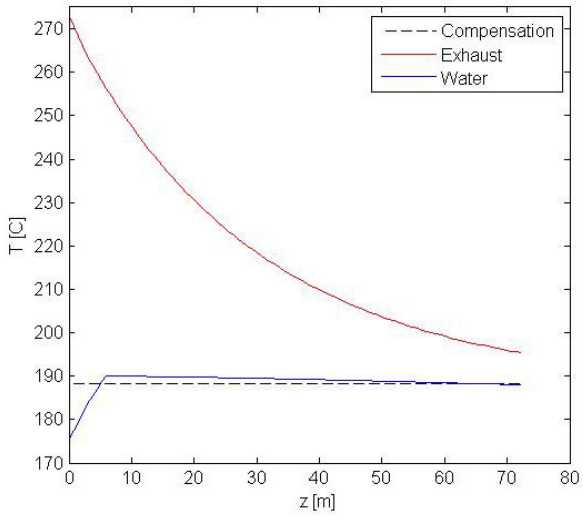

Figure 1.6: Example of pressure loss compensation

As it can be seen the use of the dotted line instead of a horizontal line at 175 °C results in a lower temperature difference for every point in the boiler, which means a lower overall heat transmission.

2. Study case: description of the boiler and system

2.1 Boiler choice

A particular real boiler on which to base the construction of the model has to be chosen. Data from the boiler (just the evaporator) installed in the WHR system on board a container ship [1] has been provided [6], with enough information on the boiler geometry and on its working parameters to make it suitable for this study.

Table 2.1 shows all the provided working parameters:

Exhaust gas flow	=	257000	kg/h
T_{gas_in}	=	273	°C
Exhaust gas pressure	≈	1	atm
Steam mass flow	=	11700	kg/h
Circulation mass flow in evaporator	=	70200	kg/h
Feedwater temperature to system	≃	173	°C
Fedwater pressure to system	≃	9.25	bar absolute
P_{sat} in evaporator	≃	9.25	bar absolute
Allowable exhaust gas pressure loss	≃	1150	Pa
Exhaust gas resistance factor per tube layer	=	0.363	-
Allowable water side pressure loss	≃	50000	Pa
Friction factor in the tubes	≃	0.02	-
Resistance factor for each bend, ζ	≃	1.0	-

Table 2.1: Container ship's WHR evaporator design data

The geometry of the evaporator is specified in Table 2.2:

Number of tubes wide, z_B	=	48	-
Number of tubes high, z_H	=	36	-
Number of water ways	=	96 (=2x48)	-
Tube length, L_{tube}	=	4005	mm
Specific heating surface, Fh	=	0.637	m^2/m tube
Specific free gas area, Fg	=	0.03278	m^2/m tube

Table 2.2: Boiler geometry data

[1] 4000 TEU capacity container ship. Length=318.24m, Beam=42.80m, Draft=14.02m; 54MW diesel engine, Max. speed=25 knots

Figure 2.1 shows a sketch of the evaporator, picturing the tube layers and their arrangement and the boiler size:

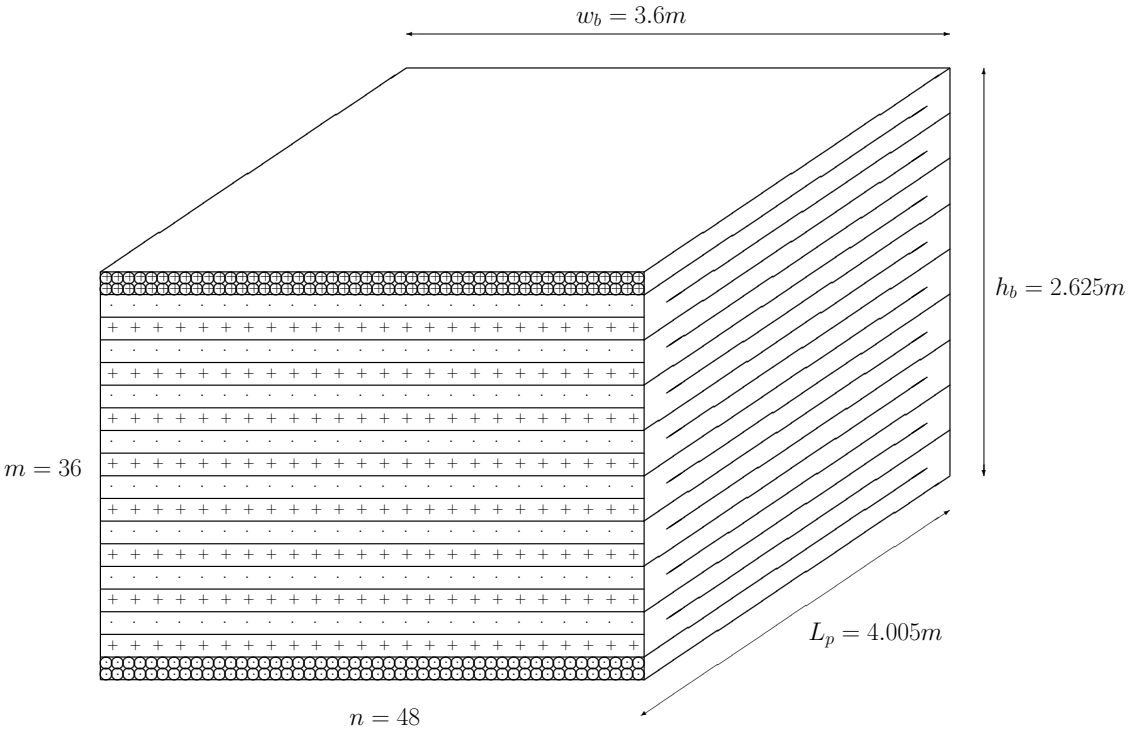

Figure 2.1: Boiler geometry

2.2 From a real WHR system to an approachable system

A WHR system is a complex system that includes many more components than the boiler and it would exceed the purpose and reach of this project to take them all into account for the development of the model.

Figure 1.2 shows an already simplified sketch of a typical single pressure marine WHR system, as it is described in section 1.4.2 of the introduction.

For the construction of the evaporator model an even simpler system, containing only the essential components is to be considered. For this purpose both the pre-heater and the super-heater are eliminated from the system and the steam line feeding the turbine and going through the condenser is neglected too. A system without the mentioned elements would look like the one in Figure 2.2.

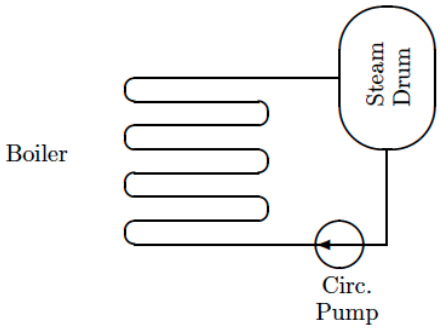

Figure 2.2: Elements of interest of the WHR system

As the main purpose of the project is the rigorous study of the pressure and temperature profile along the boiler, and it is highly affected by the relative positions of the circulation pump, drum and boiler in the system, these need to be defined.

A transversal section of a container ship engine room and casing arrangement can be seen in Figure 2.3, showing the placement of the drum and boiler in the ship's smoke stack and the pump in the engine room.

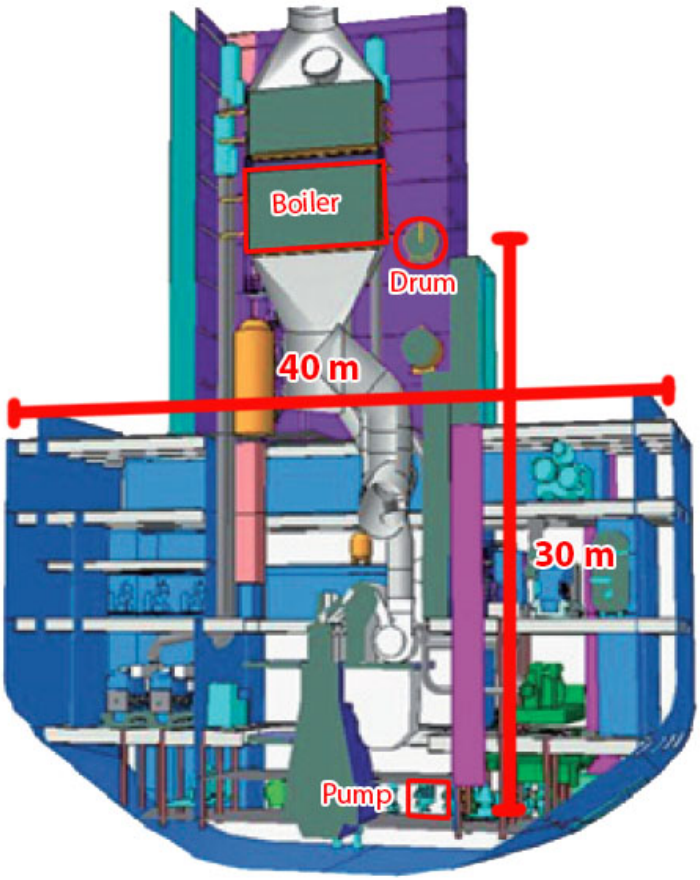

Figure 2.3: Container ship transversal section, showing the position of the boiler, drum and circulation pump [3]

Finally, taking these numbers into account, the system can be simplified as in Figure 2.4.

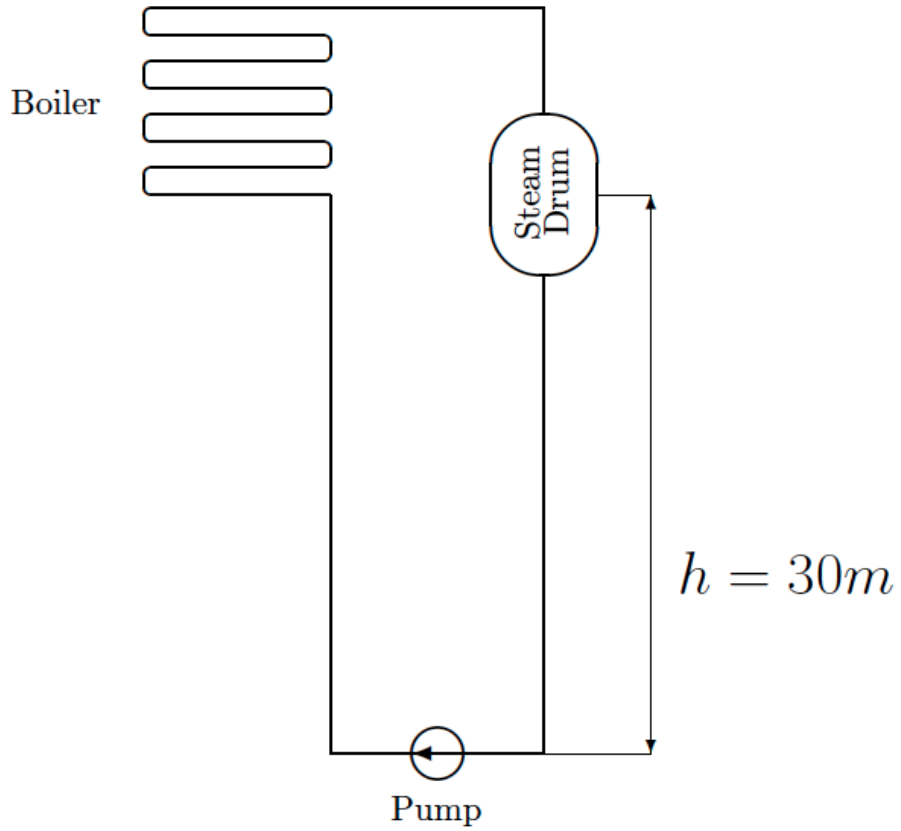

Figure 2.4: System sketch showing the relative position of the elements in the simplified system

3. Model formulation

3.1 Introduction

This chapter deals with the development of the computer models and their formulation, offering a step-by-step description of all the required equations and the parameters and variables that appear in them.

The first part of the chapter details the simplification of the boiler geometry into one that can be more easily modeled. Then a description of the basic parameters and heat balance equation, required for all the following calculations, is offered. The last section of the chapter deals with the evaluation of the pressure loss across the boiler and how this is done in an analytical and numerical way for two different two-phase flow theories.

3.2 Boiler geometry simplification

Once the system to be studied is chosen and described (section 2.1) it is necessary to simplify the complex bundle of tubes and fins that shape the boiler into a geometry for which two-phase flow equations can be written.

It is a fair assumption to consider a single pipe the length of which is that that a control volume has to travel since it enters the evaporator in the bottom, until it leaves it from the top, with an inclination that results in the same attained height and model the boiler as 96 pipes of this kind working in parallel[1] (Figure 2.1). In this manner, results for the boiler can be simply obtained by multiplying those obtained from the calculations for a single pipe by the number of waterways. The influence of the bends, which are eliminated in this simplification, is taken into account by adding an extra component to the calculation of the friction factor (see Appendix A):

$$f = f_{fric} + f_{bend} \tag{3.1}$$

$$f_{bend} = n_{bends}\,\zeta\,\frac{d}{L} \tag{3.2}$$

with n_{bends} the number of bends, ζ the resistance factor for each bend, d the pipe diameter and L the pipe length:

$$f_{bend} = 18[bends] \times 1 \times \frac{0.03[m]}{72.09[m]} = 0.0749 \tag{3.3}$$

[1] The number of pipes running in parallel is equal to the number of waterways, or tubes per layer, in the boiler, that is 48 tubes wide x 2 pipes high per layer = 96 waterways

The real geometry of the boiler is shown in Figure 2.1 in section 2.1.

The length of the pipe is calculated from equation 3.4 and given in equation 3.5:

$$\text{Pipe length} = \frac{\text{tube length} \times \text{number of tubes high}}{\text{tubes high per layer}}, \text{ then:} \tag{3.4}$$

$$L = \frac{L_p\, m}{2} = \frac{4.005[m] \times 36[tubes]}{2[tubes]} = 72.09m \tag{3.5}$$

And the inclination angle from equation 3.6:

$$\theta = \sin^{-1}\frac{h_b}{L} = \sin^{-1}\frac{2.625[m]}{72.09[m]} = 2.09^\circ \tag{3.6}$$

Which results in the configuration shown in Figure 3.1.

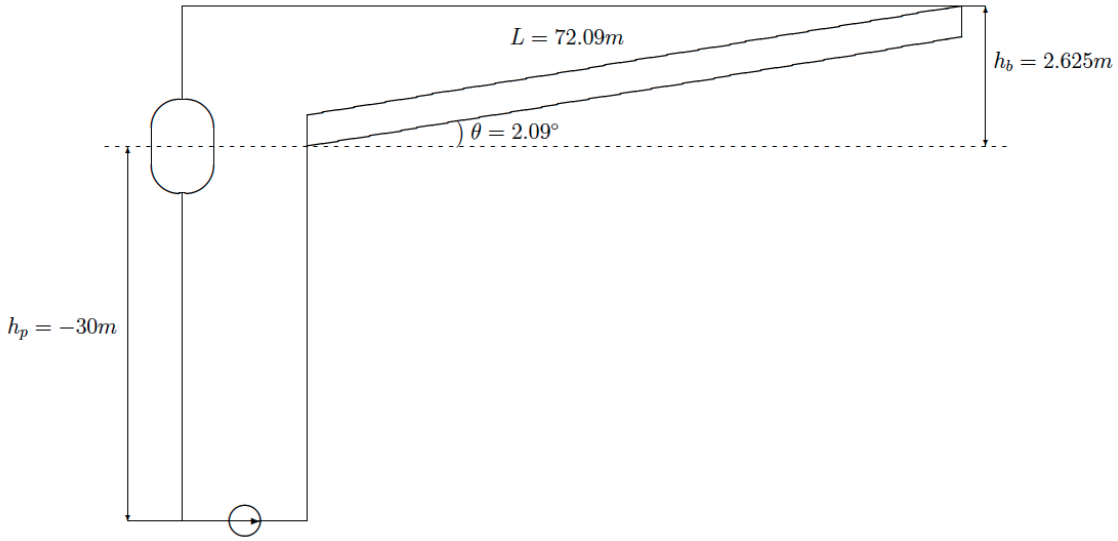

Figure 3.1: Single-pipe simplification sketch

3.3 Basic parameters

The heat transfer rate is obtained from the application of the logarithmic mean temperature difference method for a co-current heat exchanger. In order to use this method the exhaust gas properties, boiler surface areas and heat transfer coefficients need to be calculated.

The following subsections detail how these basic parameters, required to establish the heat balance, are calculated.

3.3.1 Exhaust gas data

Provided data [6] from the NASA CEA[2] computer program for the combustion of an air-fuel equivalence ratio of $\lambda = 3$ mixture of a heavy fuel with the composition shown in Table 3.1 is used to calculate the main exhaust gas properties: enthalpy h_{exh}, density ρ_{exh}, specific heat capacities c_{pexh}, c_{vexh}, viscosity μ_{exh} and thermal conductivity λ_{exh}, as a function of the exhaust gas temperature T_{exh}.

Component	Mass %
Carbon	86.6
Hydrogen	11.0
Nitrogen	0.86
Sulphur	1.81

Table 3.1: Heavy fuel composition

A table with the provided CEA data, including the exhaust gas composition, can be found in Appendix B.

3.3.2 Surface areas

The internal surface area of the boiler A_{int} is obtained from equation 3.7:

$$A_{int} = \pi \, d \, L \, n_{ww} \tag{3.7}$$

where d is the internal pipe diameter, L the pipe length and n_{ww} the number of waterways.

The total external heating surface area of the boiler A_{ext} is calculated from equation 3.8:

$$A_{ext} = L \, n_{ww} \, F_h \tag{3.8}$$

where F_h is the specific heating surface per meter of tube.

The free gas area between the tubes A_g is:

$$A_g = L_{tube} \, n \, F_g \tag{3.9}$$

where L_{tube} is the tube length, n the number of tubes wide and F_g the free gas area per meter of tube.

[2]CEA (Chemical Equilibrium with Applications) is a program which calculates chemical equilibrium product concentrations from any set of reactants and determines thermodynamic and transport properties for the product mixture. [7]

3.3.3 Heat transfer coefficients

The external convective heat transfer coefficient α_{ext} is assumed to be constant and can be calculated from equation 3.10 [3][6]:

$$\alpha_{ext} = 10.9\sqrt{V_{exh}} \tag{3.10}$$

where V_{exh} is the velocity of the exhaust gas between the tubes and can be obtained from equation 3.11 [6]:

$$V_{exh} = \frac{\dot{m}_{exh}}{A_g\,\bar{\rho}_{exh}} \tag{3.11}$$

where $\dot{m}_{exh}$ is the exhaust gas mass flow and $\bar{\rho}_{exh}$ is the mean exhaust gas density[4] between the inlet, ρ_{exh_i}, and the outlet, ρ_{exh_o}:

$$\bar{\rho}_{exh} = \frac{\rho_{exh_i} + \rho_{exh_o}}{2} \tag{3.12}$$

The internal convective heat transfer coefficient α_{int} is assumed to be constant and with a value of $\alpha_{int} = 10000\ [W/m^2K]$ as it is an usual value found in tables in literature [8], [9] for forced convection boiling and it has so little influence in the overall heat transfer coefficient that its calculation is not included in the models.

A detailed calculation of the internal heat transfer coefficient can be found in Appendix E.

Once α_{ext} and α_{int} are obtained and if the conduction resistance through the pipe walls neglected (which is a fair assumption, since the tubes have a thin wall and high thermal conductivity), the overall external heat transfer coefficient U_{ext} can be calculated as in equation 3.13:

$$U_{ext} = \frac{1}{\frac{1}{\alpha_{int}}\left(\frac{A_{ext}}{A_{int}}\right) + \frac{1}{\alpha_{ext}}} \tag{3.13}$$

[3]Equation 3.10 is a rule-of-thumb equation used in boiler design industry for its ease of use and reasonable accuracy. In reality it is an approximation of the proper calculation of the heat transfer coefficient, as a function of a Nusselt number: $Nu = \frac{\alpha\, d}{\lambda}$, which at the same time is obtained from correlations of the form $Nu = C\,Re^{0.6}\,Pr^{0.3}$ with C a constant and Re and Pr the Reynolds and Prandtl numbers respectively.

[4]A more accurate way of calculating the mean density is given in this expression:

$$\bar{\rho} = \frac{\int_{T_1}^{T_2} \rho(T)\,dT}{T_2 - T_1}$$

but is not implemented in the model because EES has problems dealing with many integrals at the same time and there are some other more important ones to be written in the code.

3.3.4 Heat balance

The use of the logarithmic mean temperature difference method allows to establish three different equations for the heat exhange from the exhaust gas to the water flow inside the boiler:

The heat transferred by the exhaust gas flow Q_{exh} can be written as in equation 3.14:

$$Q_{exh} = \dot{m}_{exh}\, c_{p_{exh}}\, \Delta T_{exh} \tag{3.14}$$

where $\dot{m}_{exh}$ is the exhaust gas mass flow, $c_{p_{exh}}$ the exhaust gas specific heat capacity at constant pressure and $\Delta T_{exh} = T_{exh_o} - T_{exh_i}$ the decrease in exhaust gas temperature across the boiler.

The heat received by the water flow Q_w is given in equation 3.15:

$$Q_w = \dot{m}_w\, \Delta h_w \tag{3.15}$$

where $\dot{m}_w$ is the mass flow inside the boiler, and $\Delta h_w = h_{w_o} - h_{w_i}$ the increase in enthalpy of the two-phase flow.

Also, the heat transfer through the pipe $Q_{T_{lm}}$ can be expressed in terms of the overall external heat transfer coefficient U_{ext}, the total heating surface A_{ext} and the logarithmic mean temperature difference for a co-current heat exchanger ΔT_{lm}:

$$Q_{T_{lm}} = U_{ext}\, A_{ext}\, \Delta T_{lm} \tag{3.16}$$

with:

$$\Delta T_{lm} = \frac{(T_{exh_i} - T_{w_i}) - (T_{exh_o} - T_{w_o})}{ln\left(\frac{T_{exh_i} - T_{w_i}}{T_{exh_o} - T_{w_o}}\right)} \tag{3.17}$$

where T_{exh_i}, T_{exh_o}, T_{w_i}, T_{w_o} are the temperatures of the exhaust gas and the two-phase flow at the inlet and the outlet of the boiler respectively.

Since there are no other heat sources or sinks, these three heat flows have to be the same and the heat balance can be established (equation 3.19):

$$-Q_{exh} = Q_w = Q_{T_{lm}} = Q \tag{3.18}$$

It should be noted here that these total heat transfers, in watts can be expressed as heat transfer rates, in watts per meter, if divided by the pipe length and both the totals and the rates[5] are implemented in the code:

[5]The heat transfer rate as shown in equation 3.19 is an average value, note that $\dot{Q} = \dot{Q}(x)$

(3.19) $$\dot{Q} = \frac{Q}{L}$$

3.4 Pressure loss evaluation: two different models

As introduced in section 1.5 three different approaches for the study of the two-phase flow have been devised: the homogeneous flow model, the separated flow model and the flow maps [5], [4]. In the following sections the implementation of the first two analysis strategies into the computer model is explained, detailing the required equations, the assumptions made along the way and the limitations found in the software. The results obtained from the homogeneous and separated flow models are then used in chapter 4 to determine the flow patterns with the help of the flow maps theory.

For each of these two ways of studying the two-phase flow both an analytical and a numerical model are built, in order to have two comparable sets of results which reflect, respectively, a direct application of the equations, which gives a fast and direct result; and a more elaborate use of the equations, which gives a more precise final result and permits the elaboration of pressure, temperature, quality and heat transfer rate profiles, as these variables are calculated for several points along the length of the pipe [10].

The following sections deal with the calculation of the pressure gradient in the sub-cooled section of the pipe and the models for the evaporating (two-phase flow) section of the boiler.

3.5 Pressure gradient in the sub-cooled section

The water enters the pipe as sub-cooled water and needs to travel a length of pipe z_{sc} to raise its temperature to saturation. This sub-cooled pipe length is given by equation 3.20, where linear heat input is assumed:

(3.20) $$\frac{z_{sc}}{L} = \frac{h_l - h_i}{\Delta h}$$

with h_l the enthalpy of saturated water, h_i the enthapy of the inlet water and Δh the enthalpy rise over the entire pipe length.

The evaporation length of the pipe is then simply obtained as the difference between the total length L and the sub-cooled section length z_{sc}:

(3.21) $$L_{ev} = L - z_{sc}$$

The pressure loss in this preheating section is the sum of the pressure loss due to friction, the pressure loss due to the acceleration of the water as a result of the change in density and the gravitational pressure loss (3.22), these three quantities are obtained from equations 3.23, 3.24 and 3.25:

$$\Delta P_{sc} = \Delta P_{sc_f} + \Delta P_{sc_a} + \Delta P_{sc_g} \tag{3.22}$$

$$\Delta P_{sc_f} = f \frac{z_{sc}}{d} \frac{G^2}{2\,\rho_m} \tag{3.23}$$

where the mean density ρ_m is the arithmetic mean of the water densities at the entrance of the pipe and at the point where it has just reached saturation temperature and the friction factor f and the mass flux G are as defined in section 3.6.

$$\Delta P_{sc_a} = G^2 \left(\frac{1}{\rho_l} - \frac{1}{\rho_{in}} \right) \tag{3.24}$$

where ρ_{in} is the density of the inlet water.

$$\Delta P_{sc_g} = \rho_m \, g \, \sin\theta z_{sc} \tag{3.25}$$

This sub-cooled pressure loss calculation is valid for all of the following models.

3.6 Pressure gradient in the evaporating section: homogeneous flow

The idea of this approach is to consider the two phases as a perfectly mixed single phase with weighed average fluid properties. The main assumptions on which the model is based are that the velocities of the liquid and the gas phase are the same, there is thermodynamic equilibrium between the phases and that a properly defined single-phase friction factor can be used. [5], [4]

The model is developed from the application of mass, momentum and energy conservation equations to a control volume like the one in Figure 3.2 and evaluating each term, but it is not the purpose of this paper to detail this derivation and only the final equations are offered.

Neglecting the compressibility of the liquid and gas phase, the pressure gradient for a steady-state flow in a constant cross section pipe is given by equation 3.26:

$$-\frac{dp}{dz} = \frac{f\,G^2}{2\,d\,\rho_h} + g\,\rho_h \, \sin\theta + G^2 \, \frac{d}{dz} \left(\frac{1}{\rho_h} \right) \tag{3.26}$$

where p is the pressure, z the horizontal coordinate, f the Darcy friction factor, G the mass flux, d the internal pipe diameter, ρ_h the homogenous density, g the acceleration of gravity and θ the pipe incline.

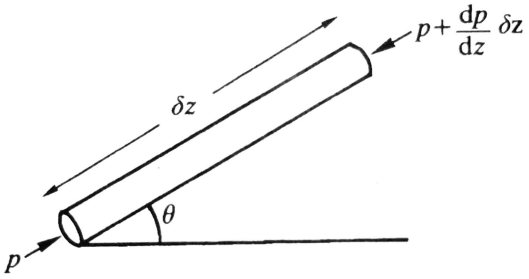

Figure 3.2: Control volume for the application of conservation equations [4]

In this expression the first term on the right represents the frictional pressure loss, the second the gravitational and the third the accelerational.

The intervening variables are defined in the following equations:

- Mass flux:

$$G = \frac{\dot{m}}{A} \tag{3.27}$$

  where $\dot{m}$ is the mass flow through the pipe and A the cross section area.
- Homogeneous density:

$$\frac{1}{\rho_h} = x\left(\frac{1}{\rho_g}\right) + (1-x)\left(\frac{1}{\rho_l}\right) \tag{3.28}$$

  where x is the quality and ρ_g and ρ_l are the densities of the saturated gas and liquid phase respectively.
- Friction factor: The friction factor f is composed of that obtained from the Colebrook-White equation (3.29) and that obtained from the bend simplification, as shown in equation 3.1. It is understood from now on in this report that any friction factor takes that of the bends into account and this will not be explicitly specified in the friction factor definitions of the next sections [11]:

$$\frac{1}{\sqrt{f_{fric}}} = 1.14 - 2\,log_{10}\left[\frac{k}{d} + \frac{9.35}{Re}\left(\frac{1}{\sqrt{f_{fric}}}\right)\right] \tag{3.29}$$

  where k is the pipe relative roughness andRe is the Reynolds number, defined as:

$$Re = \frac{G\,d}{\eta_h} \tag{3.30}$$

  and the homogeneous dynamic viscosity η_h is defined in an analogous manner to that of the homogeneous density:

(3.31) $$\frac{1}{\eta_h} = x\left(\frac{1}{\eta_g}\right) + (1-x)\left(\frac{1}{\eta_l}\right)$$

with η_g and η_l the dynamic viscosities of the saturated gas and the liquid phase respectively.

3.6.1 Analytical homogenous flow model

Assuming linear evaporation along a pipe, from an inlet quality of zero to an outlet quality x_o (equation 3.32), direct integration of (3.26) results in expression 3.33:

(3.32) $$x = \frac{x_o}{L_{ev}}\, z$$

(3.33) $$\Delta P_{ev} = \frac{f\, G^2\, L_{ev}}{2\, d}\left(\frac{x_o}{2\,\rho_g} + \frac{1}{\rho_l} - \frac{x_o}{2\,\rho_l}\right) + \frac{g\, \sin\theta\, \rho_g\, \rho_l\, L_{ev}}{x_o\,(\rho_l - \rho_g)}\, ln\left(\frac{x_o\,(\rho_l - \rho_g) + \rho_g}{\rho_g}\right) + \\ + G^2\, x_o\left(\frac{1}{\rho_g} - \frac{1}{\rho_l}\right)$$

Equation 3.33 is the expression used to evaluate the pressure loss along the length of the pipe in which evaporation occurs; where, again, the first term of the pressure change accounts for the frictional pressure loss, the second accounts for the gravitational and the third for the accelerational.

The total pressure loss along the boiler is finally obtained as the sum of the sub-cooled pressure loss and the evaporating pressure loss:

(3.34) $$\Delta P = \Delta P_{sc} + \Delta P_{ev}$$

3.6.2 Numerical homogeneous flow model

The DUPLICATE function in EES can be used for the construction of an explicit numerical model[6] in which the value of each variable is calculated based on its value in the previous element, and the derivatives are approximated taking backward finite differences.

The pipe is divided in n_{steps} equal differential elements like the one in Figure 3.2. The size of the elements z_{step} is simply obtained dividing the pipe length L by the number of elements.

(3.35) $$z_{step} = \frac{L}{n_{steps}}$$

[6]It is important to note here that although explicit numerical methods are not unconditionally stable a convergence study carried out from a number of elements ranging from 219 to 2 proves that the built model is stable, as shown in Appendix C

The position of each element in the boiler z_i is the position of the previous element z_{i-1} plus the element size z_{step} :

$$z_i = z_{i-1} + z_{step} \tag{3.36}$$

Inlet properties for each pipe segment are defined as the outlet properties of the previous one.

The absolute pressure for each pipe segment is obtained in this manner:

$$p_i = p_{i-1} + \Delta p_i \tag{3.37}$$

where the pressure change Δp_i in equation 3.37 is evaluated from equation 3.26:

$$\Delta P_i = \Delta P_{i_f} + \Delta P_{i_g} + \Delta P_{i_a} \tag{3.38}$$

$$\Delta P_{i_f} = \frac{f_{i-1}\, z_{step}\, G^2}{2\, d\, \bar{\rho}_{h_i}} \tag{3.39}$$

$$\Delta P_{i_g} = g\, \bar{\rho}_{h_i}\, \sin\theta\, z_{step} \tag{3.40}$$

$$\Delta P_{i_a} = G^2\, \frac{d}{dz}\left(\frac{1}{\rho_h}\right) = G^2 \left(\frac{1}{\rho_{h_i}} - \frac{1}{\rho_{h_{i-1}}}\right) \tag{3.41}$$

The mean density $\bar{\rho}_i$ used for the frictional and gravitational pressure changes in each element is defined as the arithmetical mean between the inlet ρ_{i-1} and the outlet density ρ_i:

$$\bar{\rho}_i = \frac{\rho_{i-1} + \rho_i}{2} \tag{3.42}$$

The overall pressure loss along the length of the pipe is finally obtained as the sum of the sub-cooled section pressure loss and the sum of the pressure loss of all the elements:

$$\Delta P = \Delta P_{sc} + \sum_{i=1}^{n_{steps}} \Delta P_i \tag{3.43}$$

3.7 Separated flow model

The separated flow model considers that both phases are segregated in the pipe and flow with different velocities, as seen schematically in Figure 3.3:

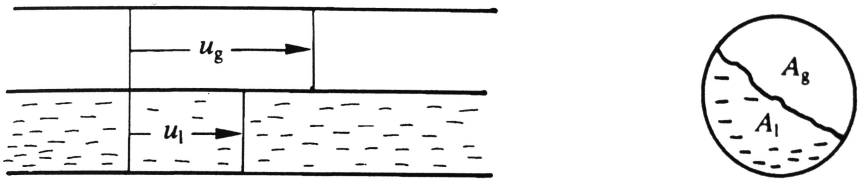

Figure 3.3: Separated two-phase flow [4]

Assuming thermodynamic equilibrium between the phases, the momentum conservation equation can be applied to a control volume like the one in Figure 3.4:

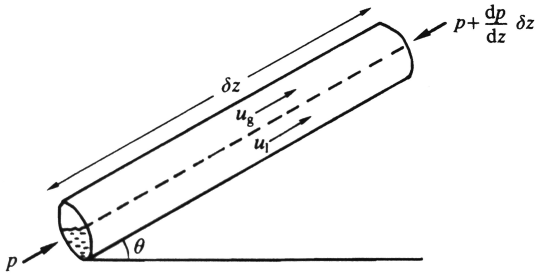

Figure 3.4: Control volume for the application of the momentum conservation equation [4]

If the compressibilities of the liquid and gas phases are neglected, the pressure gradient is given by equation 3.44 [4]:

$$-\frac{dp}{dz} = \frac{f_{lo}\,G^2}{2\,d\,\rho_l}\,\phi_{lo}^2 + g\,\left[\rho_g\,\alpha + \rho_l(1-\alpha)\right]\sin\theta + G^2\,\frac{d}{dz}\left[\frac{x^2}{\alpha\,\rho_g} + \frac{(1-x)^2}{(1-\alpha)\,\rho_l}\right] \tag{3.44}$$

where p is the pressure, z the horizontal coordinate, f_{lo} the Darcy friction factor for a liquid-only flow, G the mass flux, d the internal pipe diameter, ρ_l and ρ_g the liquid and gas densities respectively, ϕ_{lo}^2 the liquid-only flow multiplier, α the void fraction, g the acceleration of gravity, θ the pipe inclination and x the quality.

The new intervening variables are defined in the following equations:

Liquid-only friction factor:

The liquid-only friction factor f_{lo}, is the friction factor based on the total flow considered as liquid and is obtained in the same way than for homogeneous flow, but considering the liquid dynamic viscosity η_l in the evaluation of the Reynolds number instead of an homogeneous dynamic viscosity (equations 3.45 and 3.46):

$$f_{lo} = \frac{0.316}{Re_l^{0.25}} \tag{3.45}$$

$$Re_l = \frac{G\,d}{\eta_l} \tag{3.46}$$

Liquid-only flow multiplier:

Flow multipliers are a simple way to relate the friction based on single-phase flow to that of two-phase flow, so the two-phase flow pressure gradient can be expressed in terms of the single-phase pressure gradient for the total flow considered as liquid [5]:

$$-\left(\frac{dp}{dz}\right)_f = -\left(\frac{dp}{dz}\right)_{f_{lo}} \phi_{lo}^2 \tag{3.47}$$

The liquid-only flow multiplier is calculated from the Friedel correlation, considered to be one of the most accurate two-phase pressure drop correlations [5]:

$$\phi_{lo}^2 = E + \frac{3.24\,F\,H}{Fr^{0.045}\,We^{0.035}} \tag{3.48}$$

with:

$$E = (1-x)^2 + x^2 \frac{\rho_l\,C_{fgo}}{\rho_g\,C_{flo}} \tag{3.49}$$

C_{fgo} and C_{flo} being the friction factors[7] for the total mass flux flowing with the gas and liquid properties respectively (obtained as in equations 3.45 and 3.46);

$$F = x^{0.78}(1-x)^{0.224} \tag{3.50}$$

$$H = \left(\frac{\rho_l}{\rho_g}\right)^{0.91} \left(\frac{\mu_g}{\mu_l}\right)^{0.19} \left(1 - \frac{\mu_g}{\mu_l}\right)^{0.7} \tag{3.51}$$

and Fr and We the Froude and Weber dimensionless numbers respectively:

[7] For the sake of consistency with the notation in the Friedel correlation the friction factors are expressed here as C_{fgo} and C_{flo} instead of with the letter f, which is the symbol used for friction factors everywhere else in this paper.

$$Fr = \frac{G^2}{g\, d\, \rho_h^2} \tag{3.52}$$

$$We = \frac{G^2\, d}{\sigma\, \rho_h} \tag{3.53}$$

σ being the water surface tension and ρ_h the homogeneous density as defined in equation 3.28.

Void fraction:

The void fraction α is defined as the instantaneous area of a channel occupied by the gas phase divided by the cross sectional area of the channel:

$$\alpha = \frac{A_g}{A_{total}} \tag{3.54}$$

or:

$$(1 - \alpha) = \frac{A_l}{A_{total}} \tag{3.55}$$

In general, the area any of the phases is occupying is unknown unless it is meassured and the void fraction needs to be obtained from empirical correlations. The CISE correlation offers α in terms of the slip ratio S, which is the actual velocity ratio between the gas and the liquid phase (u_g/u_l):

$$\alpha = \frac{1}{1 + \left(S\, \frac{1-x}{x}\, \frac{\rho_g}{\rho_l} \right)} \tag{3.56}$$

The slip ratio S is given by:

$$S = 1 + E_1 \left(\frac{y}{1 + y\, E_2} - y\, E_2 \right)^{0.5} \tag{3.57}$$

where

$$y = \frac{\beta}{1 - \beta} \tag{3.58}$$

(3.59) $$\beta = \frac{\rho_l \, x}{\rho_l \, x + \rho_g (1 - x)}$$

(3.60) $$E_1 = 1.578 \, Re^{-0.19} \left(\frac{\rho_l}{\rho_g} \right)^{0.22}$$

(3.61) $$E_2 = 0.0273 \, We_l \, Re^{-0.51} \left(\frac{\rho_l}{\rho_g} \right)^{-0.08}$$

and Re_l and We_l are the Reynolds (as defined in equation 3.46) and Weber numbers for the flow considered as liquid only:

(3.62) $$We_l = \frac{G^2 \, d}{\sigma \, \rho_l}$$

3.7.1 Analytical separated flow model

Assuming linear evaporation along a pipe, from an inlet quality of zero to an outlet quality x_o (equation 3.32), direct integration of (3.44) results in expression 3.63, which is used for the evaluation of the pressure loss in the evaporating section of the pipe:

(3.63) $$\Delta P_{ev} = \frac{f_{lo} \, G^2 \, L_{ev}}{2 \, d \, \rho_l} \left[\frac{1}{x_o} \int_0^{x_o} \phi_{lo}^2 dx \right] + \frac{L_{ev} \, g \, \sin\theta}{x_o} \int_0^{x_o} [\rho_g \, \alpha + \rho_l (1 - \alpha)] dx + \\ + \frac{G^2}{\rho_l} \left[\frac{x_o^2}{\alpha} \left(\frac{\rho_l}{\rho_g} \right) + \frac{(1 - x_o)^2}{(1 - \alpha)} - 1 \right]$$

where the first term to the right is the frictional pressure loss, the second the gravitational and the third the accelerational.

As in the analytical homogeneous flow model, the total pressure loss is the sum of that for the sub-cooled section (as obtained in section 3.5) and that of the evaporation section of the pipe:

(3.64) $$\Delta P = \Delta P_{sc} + \Delta P_{ev}$$

3.7.2 Numerical separated flow model

As with homogenous flow, the DUPLICATE function in EES is used to build an explicit numerical model, in which the properties of the flow in one element are based in those of the previous element and derivatives are approximated by backwards finite differences.

Discretization of the pipe is done in the same manner as for the homogenous flow numerical model (equations 3.35, 3.36 and 3.37).

The three different pressure loss components are evaluated from equation 3.44 for each element:

pressure loss due to friction:

$$\Delta P_{i_f} = \frac{f_{lo_{i-1}}\, G^2\, z_{step}}{2\, d\, \bar{\rho}_{li}}\, \phi^2_{lo_i} \tag{3.65}$$

where $\phi^2_{lo_i}$ is obtained by application of the Friedel correlation for each element;

the pressure change due to gravitation:

$$\Delta P_{i_g} = g\, [\bar{\rho}_{g_i}\, \alpha_i + \bar{\rho}_{l_i}(1-\alpha_i)]\, \sin\theta\, z_{step} \tag{3.66}$$

and the pressure change due to acceleration:

$$\Delta P_{i_a} = G^2 \left[\left(\frac{x_i^2}{\alpha_i\, \rho_{g_i}} + \frac{(1-x_i)^2}{(1-\alpha_i)\, \rho_{l_i}} \right) - \left(\frac{x_{i-1}^2}{\alpha_{i-1}\, \rho_{g_{i-1}}} + \frac{(1-x_{i-1})^2}{(1-\alpha_{i-1})\, \rho_{l_{i-1}}} \right) \right] \tag{3.67}$$

where, as in the numerical homogeneous flow model, $\bar{\rho}_{g_i}$ and $\bar{\rho}_{l_i}$ are arithmetical mean densities between inlet and outlet of an element for the gas and the liquid phase respectively.

The total pressure loss for each element is given by equation 3.38 and the total pressure loss along the length of the pipe by equation 3.43, in the same manner as it is done in the numerical homogeneous flow model.

4. Results

4.1 Introduction

All the results presented in this chapter are obtained from running the EES models under the operating conditions, given in Table 4.1. The only fixed parameters of the system are the exhaust gas conditions, obtained from the boiler design data for a container ship given in Table 2.1 in chapter 2, the drum pressure, which is kept at 9 bar as it is fairly common in the marine WHR industry [3], [6]; the return pipe pressure loss from the boiler to the drum, of 0.2 bar; and the mass flow through the boiler, which has been obtained from the same provided design data (Table 2.1).

Exhaust gas mass flow	71.389	kg/s
Exhaust gas inlet temperature	273	°C
Exhaust gas pressure	104325	Pa
Water mass flow	19.5	kg/s
Drum pressure	9	bar
Return pipe pressure loss	0.2	bar

Table 4.1: Operating conditions

A comment should be made here in respect to the mass flow of water through the system and the fact that it is a fixed quantity in the models: in real systems the mass flow is actually given by the intersection of the systems characteristc curve with that of the pump. Pump curves have not been introduced in the formulation of the models and therefore a fixed mass flow has been chosen. Again, the one used for this results has been obtained from the provided data for the case study.

Results are presented below for each of the models, providing graphics for the parameters which are interesting to observe along the length of the pipe: quality, heat transfer rate, exhaust gas and water temperatures, pressure gradient and static pressure; and a table showing the total pressure loss, the inlet pressure, outlet quality, exhaust gas outlet temperature, pinch point temperature difference and total heat transfer.

At the end of the chapter these results are used to determine the different flow patterns present along the pipe with the aid of the flow maps.

4.2 Analytical homogeneous flow model

The results obtained from this model are shown in Table 4.2 and Figure 4.1:

Total pressure loss, ΔP	50355	Pa
Inlet pressure, P_{in}	9.70	bar
Outlet quality, x_o	0.168	-
Exhaust gas outlet temperature, T_{exh_o}	184.0	°C
Pinch point	7.7	K
Total heat transfer, Q	6.724	MW

Table 4.2: Analytical homogeneous flow model results

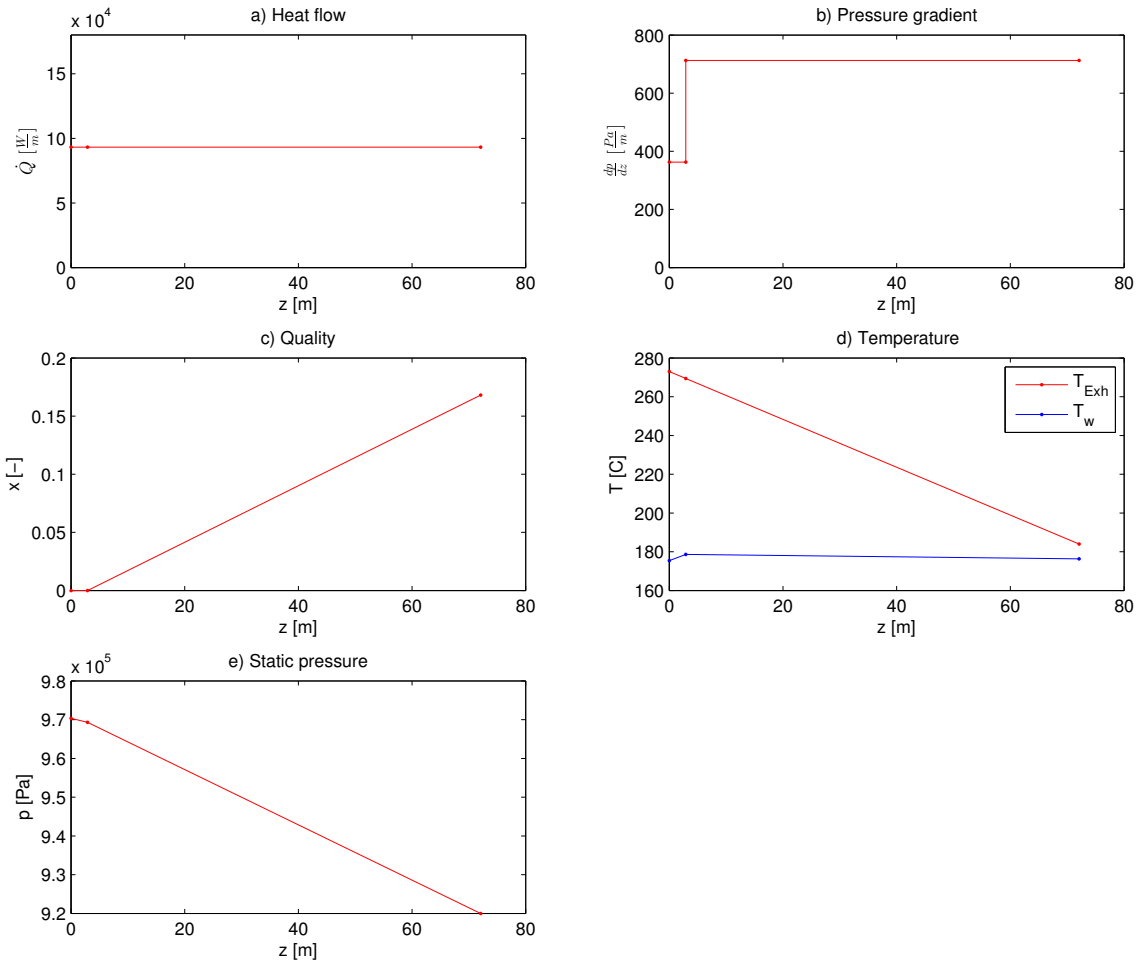

Figure 4.1: Analytical homogeneous flow model results

Quality

The analytical models assume constant heat input and therefore linear evaporation. As it can be seen in Figure 4.1(c), which shows a quality of $x = 0$ in the sub-cooled section of the pipe and a linear quality increase in the evaporation section.

Heat transfer rate

The heat transfer rate is assumed to be constant along the length of the pipe in the analytical models, as can be seen in Figure 4.1(a).

Temperatures

The exhaust gas temperature decreases linearly from inlet temperature to outlet temperature. Water temperature is observed to increase from inlet temperature to saturation temperature in the sub-cooled region and then decreasing slightly and linearly along the length of the evaporation section of the pipe. This decrease in saturation temperature is due to the pressure loss along the pipe: as the static pressure decreases in the boiler saturation temperature decreases with it too.

Pressure gradient

The pressure gradient is constant in the analytical models. As it can be seen in Figure 4.1(b) it is significantly higher in the evaporation section of the pipe, where two-phase flow effects occur, than in the sub-cooled region. These gradients are calculated as the total pressure loss in each section divided by the length of the section, therefore, there is an observed discontinuity at the end of the sub-cooled section, as the pressure gradient in the evaporation section is higher.

Static pressure

With a constant pressure gradient, the total static pressure has to decrease linearly, as observed in Figure 4.1(e).

4.3 Numerical homogeneous flow model

The results obtained from this model are offered in Table 4.3 and Figure 4.2:

Total pressure loss, ΔP	66421	Pa
Inlet pressure, P_{in}	9.86	bar
Outlet quality, x_o	0.166	-
Exhaust gas outlet temperature, T_{exh_o}	185.1	°C
Pinch point	8.8	K
Total heat transfer, Q	6.624	MW

Table 4.3: Numerical homogeneous flow model results

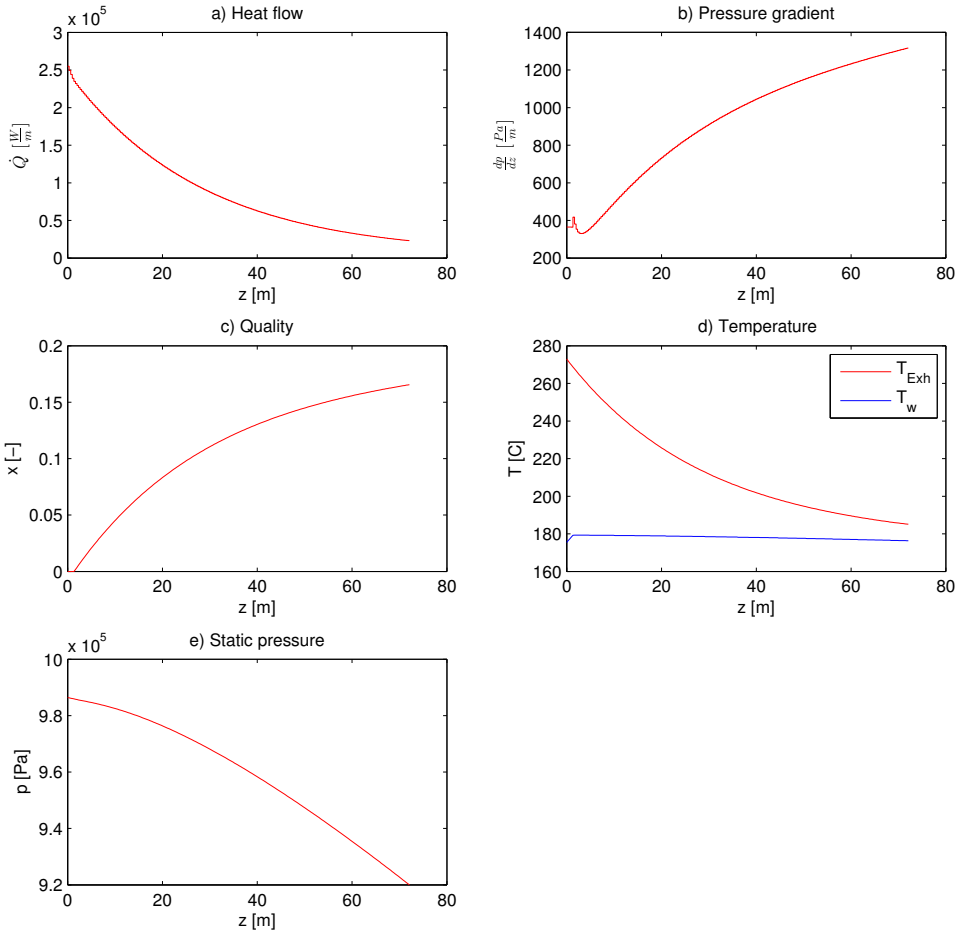

Figure 4.2: Numerical homogeneous flow model results

Quality

The quality increase rate is observed to decrease along the length of the pipe $\left(\frac{\partial^2 x}{\partial z^2} < 0\right)$.

Heat transfer rate

The power transferred per meter of pipe diminishes faster in the first meters of pipe, where evaporation occurs at a fast pace and slower in the last meters of the pipe, where evaporation happens at a much slower pace $\left(\frac{\partial^2 \dot{Q}}{\partial z^2} < 0\right)$, as seen in Figure 4.2(a).

Temperatures

Figure 4.2(d) shows a slight decrease in saturation temperature along the length of the pipe, due to the pressure loss, and a non-linear decrease in the exhaust gas temperature, with a curve that has the same shape as that for the heat transfer rate.

Pressure gradient

The pressure gradient is observed to be constant along the sub-cooled region, and jumps abruptly when evaporation starts. It then decreases rapidly to a minimum and from that point on increases along the whole length of the pipe. To understand why this happens it is necessary to decompose the pressure gradient in its three components and observe how they evolve as evaporation happens. This decomposition and analysis are done in section 4.6 of this chapter.

Static pressure

The static pressure inside the pipe decreases along the whole length, with a higher speed at the last part than at the beginning $\left(\frac{\partial^2 P}{\partial z^2} > 0\right)$.

4.4 Analytical separated flow model

The results obtained from this model are offered in Table 4.4 and Figure 4.3.

Total pressure loss, ΔP	65817	Pa
Inlet pressure, P_{in}	9.86	bar
Outlet quality, x_o	0.167	-
Exhaust gas outlet temperature, T_{exh_o}	184.0	°C
Pinch point	7.7	K
Total heat transfer, Q	6.724	MW

Table 4.4: Analytical separated flow model results

Quality

As in the analytical homogeneous flow model linear evaporation is assumed. As it can be seen in Figure 4.3(c), which shows a quality of $x = 0$ in the sub-cooled section of the pipe and a linear quality increase in the evaporation section.

Heat transfer rate

The heat transfer rate is considered to be constant for the whole length of the pipe.

Temperatures

The same tendencies as for the analytical homogeneous flow can be observed in Figure 4.3(d): the exhaust gas temperature decreases linearly from inlet temperature to outlet temperature. Water temperature is observed to increase from inlet temperature to saturation temperature in the sub-cooled region and to decrease sligthly and linearly along the length of the evaporation section of the pipe. This decrease in saturation temperature is due to the pressure loss along the pipe: as the static pressure decreases in the boiler saturation temperature decreases with it too.

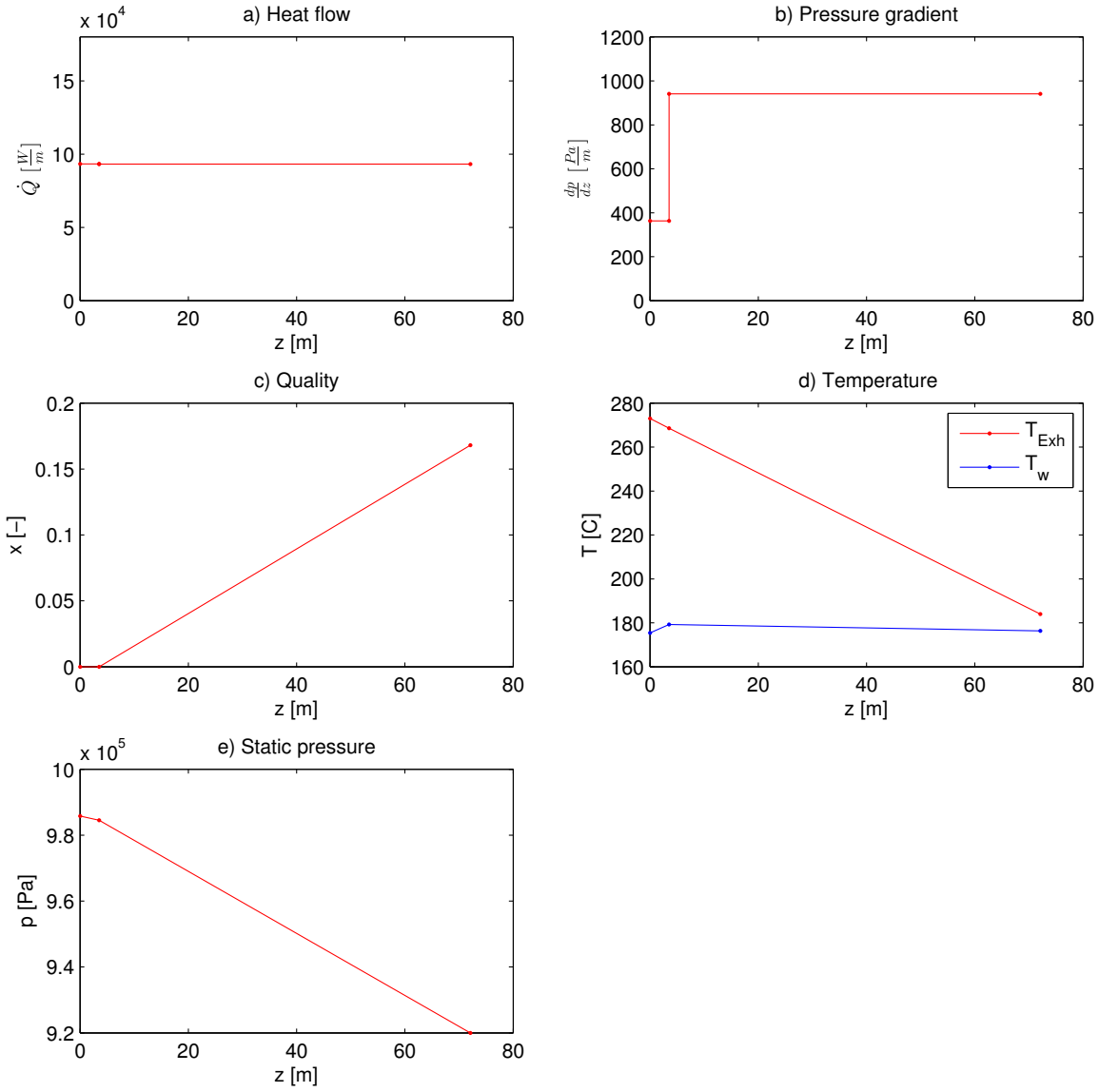

Figure 4.3: Analytical separated flow model results

Pressure gradient

The pressure gradient is constant in the sub-cooled and evaporating sections, being much higher in the evaporation one due to the two-phase flow effects.

Static pressure

With a constant pressure gradient the total static pressure is observed to decrease linearly.

4.5 Numerical separated flow model

The results obtained from this model are offered in Table 4.5 and Figure4.4.

Total pressure loss, ΔP	83193	Pa
Inlet pressure, P_{in}	10.03	bar
Outlet quality, x_o	0.165	-
Exhaust gas outlet temperature, T_{exh_o}	185.3	°C
Pinch point	9.0	K
Total heat transfer, Q	6.607	MW

Table 4.5: Numerical separated flow model results

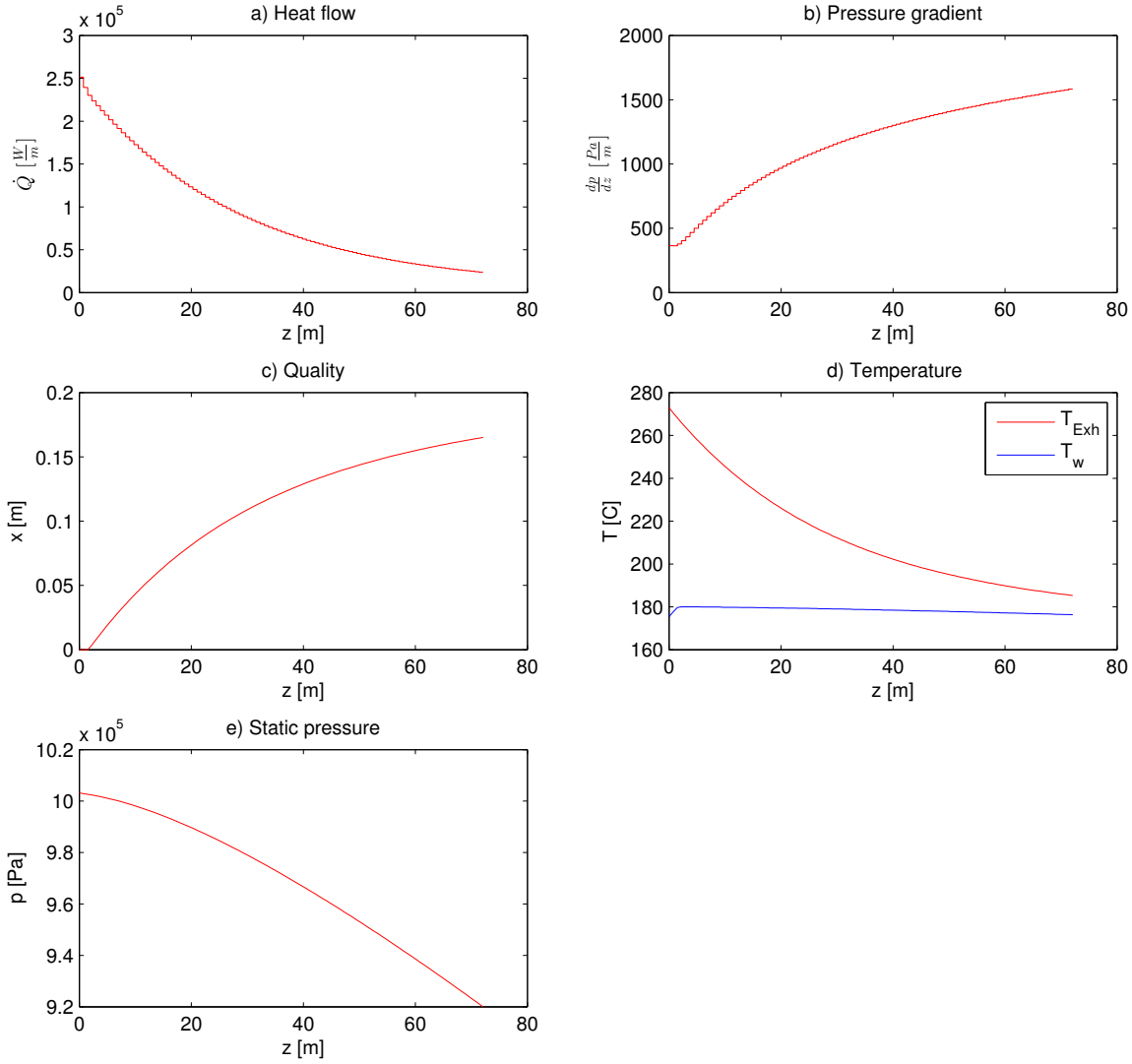

Figure 4.4: Numerical separated flow model results

Quality

The quality is observed to evolve in the same way as in the numerical homogenous flow model: faster at the beginning of the evaporation section than at the end.

Heat transfer rate

The heat transfer rate decreases along the whole length of the pipe, doing so faster in the first meters than in the last.

Temperatures

Figure 4.4(d) shows a slight decrease in saturation temperature along the length of the pipe, due to the pressure loss, and a non-linear decrease in the exhaust gas temperature, with a curve that has the same shape than that for the heat transfer rate.

Pressure gradient

The pressure gradient is constant for the sub-cooled section of the pipe and increases along the evaporation section, faster at the beginning of this section than at the end. The abrupt jump observed in the numerical homogeneous flow model is probably not observed in this one as well due to its lower resolution.

Static pressure

Static pressure decreases along the whole length of the pipe, at a higher speed in the last meters than in the first ones.

4.6 Pressure gradient composition

There is an interesting effect observed in the graphic for the pressure gradient in the numerical models. Figure 4.2(b) shows a sudden jump in the pressure gradient at the beginning of the evaporation section, after which it decreases to a minimum and then starts increasing again, along the rest of the length of the pipe.

For both models the pressure gradient has been decomposed in its three components, so each one can be observed independently.

4.6.1 Refined grid numerical homegenous flow model

In order to study this effect the grid has been refined, utilizing an increasing step size, defined as:

$$z_{step_i} = \frac{\sqrt{z_i}}{K} \tag{4.1}$$

where K is an arbitrary constant which proved to work well. This manner of defining the step size provides a higher density of steps in the first meters of pipe, where the interesting phenomena occurs, and a lower step density, with longer steps, in the last meters of pipe, where resolution has very little effect, as shown in the convergence study in Appendix C.

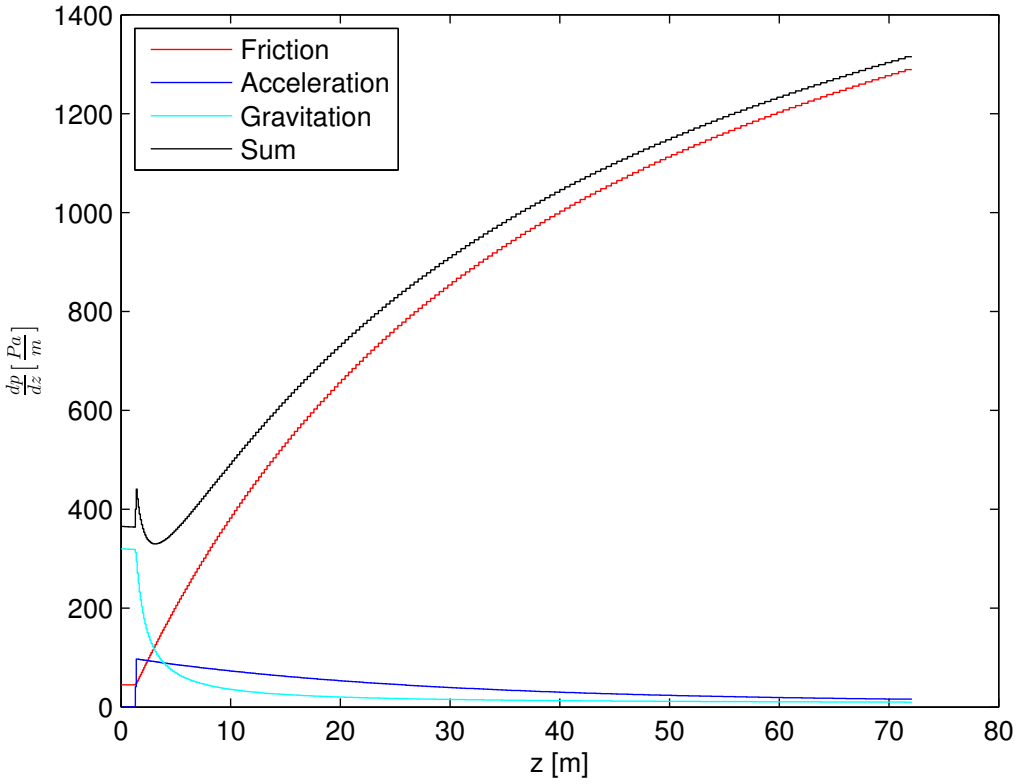

Figure 4.5: Composition of the pressure gradient

It is shown in Figure 4.5 how the accelerational pressure gradient jumps abruptly at the end of the sub-cooled section, due to the first appearance of steam accelerating the flow (a sudden decrease in density); as evaporation continues, the change in density from one step to the next gets smaller, therefore acceleration of the flow diminishes and hence the accelerational pressure gradient.

The frictional pressure gradient is constant in the sub-cooled section and increases for the whole length of the pipe, as density decreases.

The decrease in density strongly affects the gravitational pressure gradient, making it decrease abruptly as soon as evaporation begins and being almost non-existent at the end of the pipe.

The composition of these three phenemona result in the shown total pressure gradient, which has that shape because the jump in the accelerational component is higher than the decrease in the gravitational as evaporation starts and the frictional component increases slower than the other two decrease in the first meters of the evaporation section. The overall pressure gradient is observed to follow the frictional one almost perfectly after the first five meters of pipe, after which it is this component which accounts for almost all the pressure loss.

4.6.2 Refined grid numerical separated flow model

The same phenomena can be observed in the separated flow model, for which a refined grid, with very small step size has been built, in order to be able to observe the first five meters of pipe with the highest possible resolution.

As in the previous discussion, the peak, decrease and increase in the total pressure gradient can be seen to be a consequence of the accelerational jumping abruptly at the beginning of evaporation and then decreasing, as well as the gravitational part, faster than the frictional grows in the first meters of pipe; as shown in Figure 4.6:

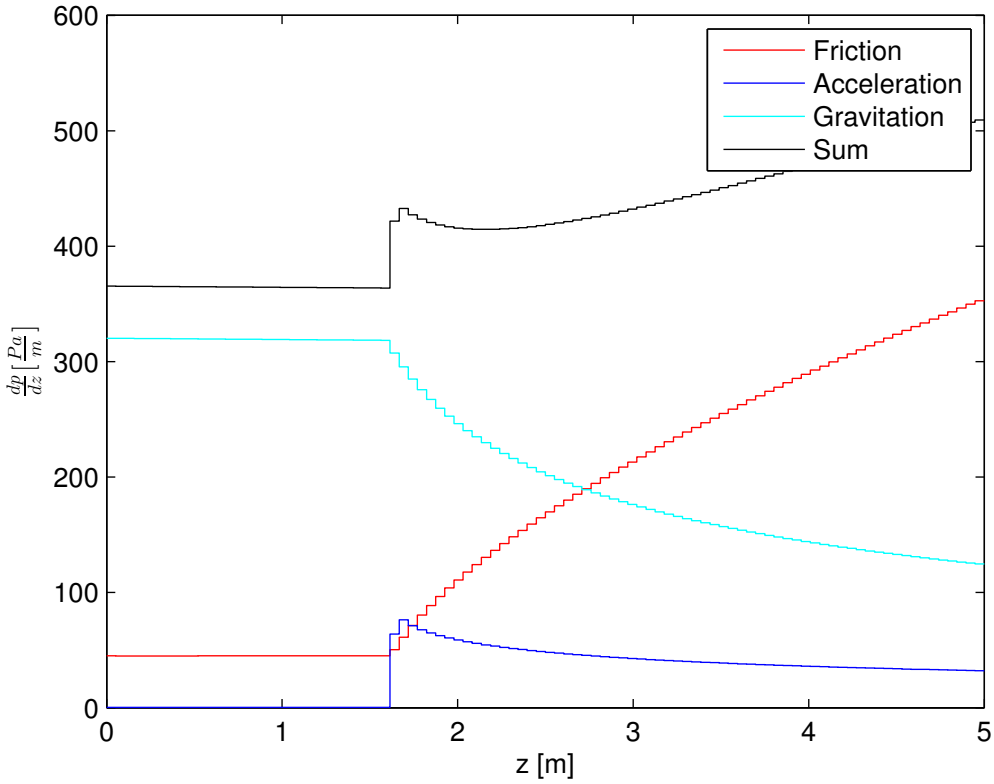

Figure 4.6: Composition of the pressure gradient

4.7 Model comparison and discussion

This section offers a comparison of the results obtained for each of the studied variables between the four different models. The differences between the models can be observed both in the figures, showing the evolution of the quality, heat transfer rate, exhaust gas and saturation temperature, pressure gradient and static pressure along the length of the pipe, and in the tables, which show the outlet quality, the total heat transfer, the exhaust gas outlet temperature, the inlet pressure, the total pressure drop and the pinch point temperature difference.

4.7.1 Quality

As it can be seen in Table 4.6, all the models give the same outlet quality, the difference between the smallest and the largest being, roughly 2%.

Model	x_o
Homogeneous analytical	0.168
Homogeneous numerical	0.166
Separated flow analytical	0.167
Separated flow numerical	0.165

Table 4.6: Outlet quality - Four models comparison

Figure 4.7 shows the evolution of the quality along the length of the pipe.

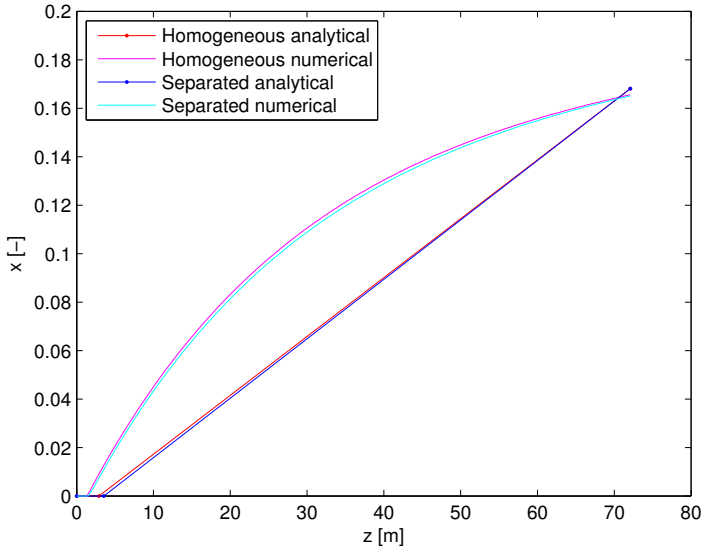

Figure 4.7: Quality - Four models comparison

Both analytical models show a linear quality increase, with the only appreciable difference being a slightly longer subcooled section in the separated flow model.

The numerical models produce curves of the exact same shape, with faster evaporation in the first meters of the boiling section than in the last ones. The homogeneous flow model gives a slightly higher quality than the separted flow one for any given point of the pipe, as it is more optimistic with the pressure loss calculation and predicts higher heat transfer rates.

4.7.2 Heat transfer rate

Table 4.7 shows the total heat transfer, while Figure 4.8 shows the evolution of the heat flux along the length of the pipe.

As it can be seen, both analytical models assume the same constant heat flux for the whole length and give the exact same amount of heat transfered. The numerical models show both the same evolution for the heat flux. The difference between the highest heat transfer, obtained from the analytical homogenous flow model, and the lowest, obtained from the numerical separated flow model, is of 0.117 MW (1.8%).

Model	Q [MW]
Homogeneous analytical	6.724
Homogeneous numerical	6.624
Separated flow analytical	6.724
Separated flow numerical	6.607

Table 4.7: Total heat transfer - Four models comparison

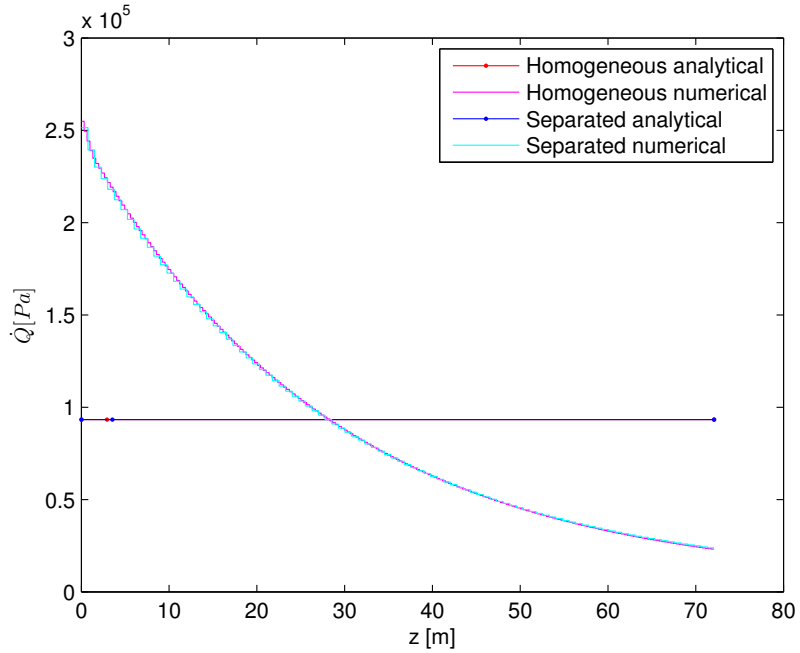

Figure 4.8: Heat flow - Four models comparison

4.7.3 Pressure gradient and static pressure

Table 4.8 shows the total pressure loss:

Model	ΔP [Pa]
Homogeneous analytical	50355.18
Homogeneous numerical	66421.96
Separated flow analytical	65817.70
Separated flow numerical	83193.49

Table 4.8: Pressure loss - Four models comparison

The numerical separated flow model shows the largest pressure loss, being almost 0.3 bar higher than that obtained with the analytical homogeneous flow model. It can be noticed too that for any of the two flow models, the numerical analysis gives a higher total pressure loss. This can be observed as well in Figure 4.9:

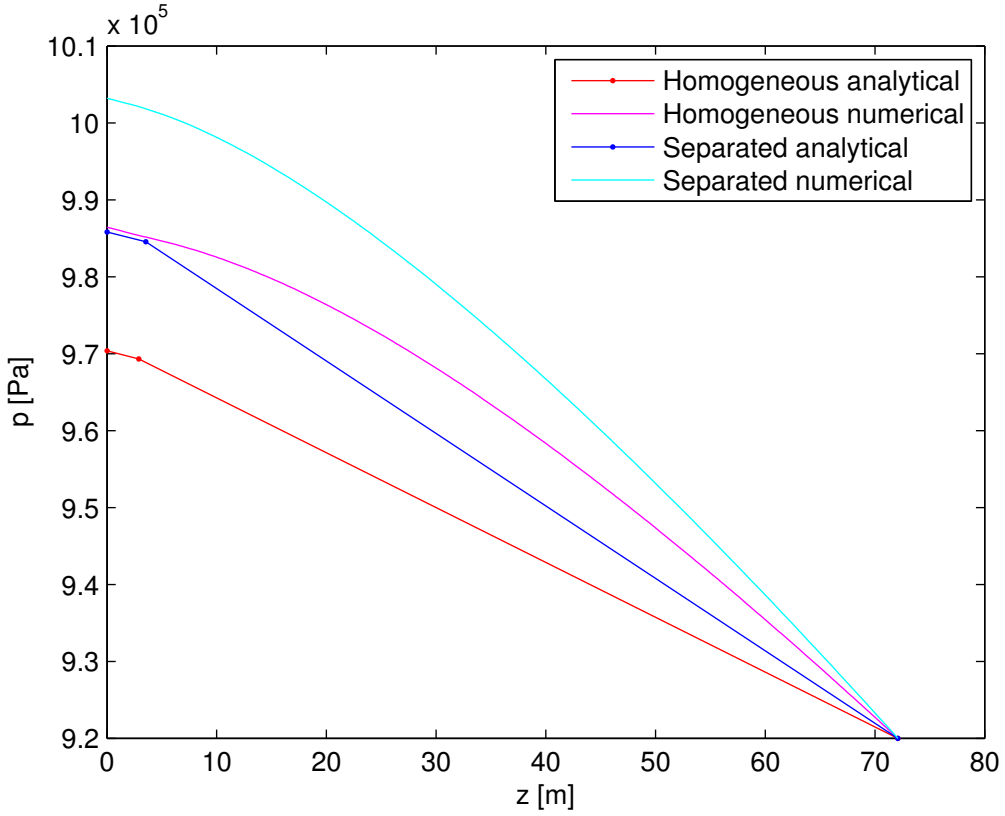

Figure 4.9: Static pressure - Four models comparison

The pressure gradient figure (Figure 4.10) shows the analytical models having constant pressure gradients, higher for the separated flow than for the homogeneous and with a slightly longer sub-cooled section for the latter.

As for the numerical models, both show the same shape, although due to the higher resolution of the homogenous flow one, the phenomena along the first meters of the

evaporation section previously described in section 4.6 can be observed for this model and not for the separated flow one. Again, separated flow results are observed to be higher along the whole length of the pipe.

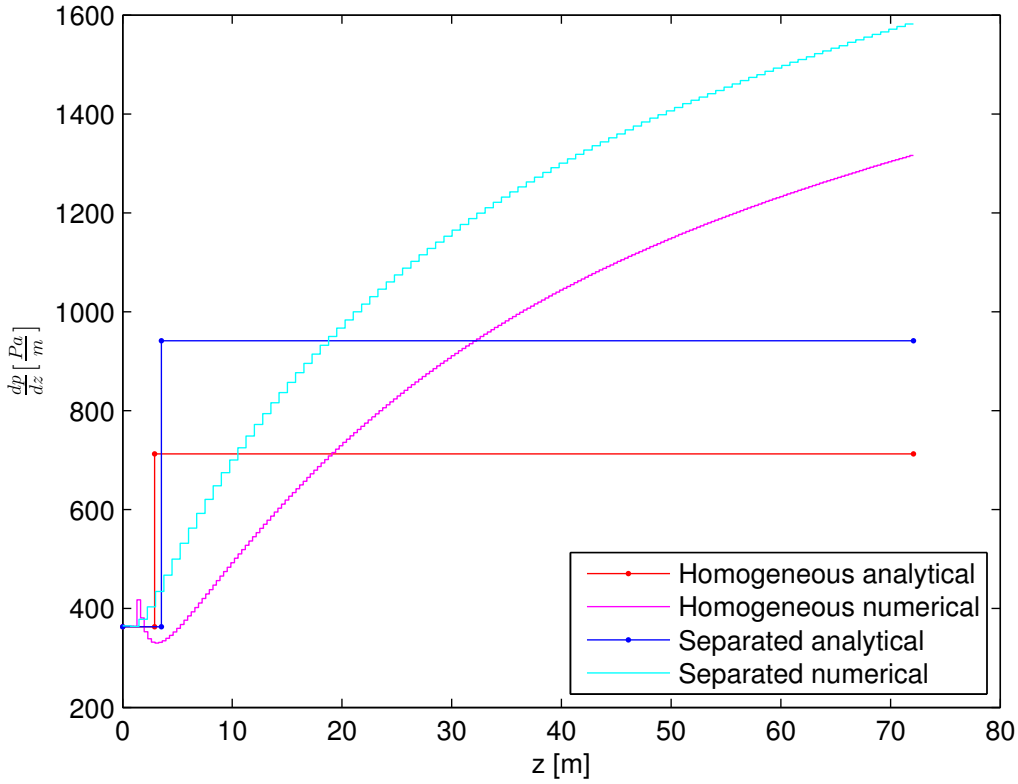

Figure 4.10: Pressure gradient - Four models comparison

4.7.4 Temperatures

Table 4.9 shows the exhaust gas outlet temperatures and the pinch point temperature differences for the four models:

Model	T_{exh_o} [°C]	Pinch point [K]
Homogeneous analytical	184.0	7.7
Homogeneous numerical	185.1	8.8
Separated flow analytical	184.0	7.7
Separated flow numerical	185.3	9.0

Table 4.9: Exhaust gas temperature and pinch point - Four models comparison

Analytical models produce the exact same result. Numerical models give a pinch point 1.1 K higher for the homogeneous flow model and 1.3 K for the separated flow model.

The evolution of the exhaust gas temperature, as well as the saturation temperature inside the pipe can be seen in Figures 4.11 and 4.12:

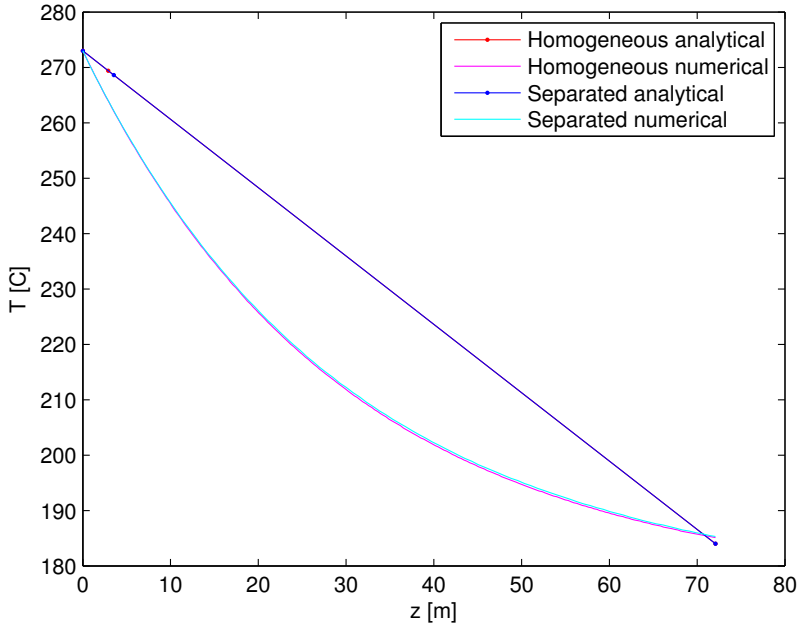

Figure 4.11: Exhaust gas temperature - Four models comparison

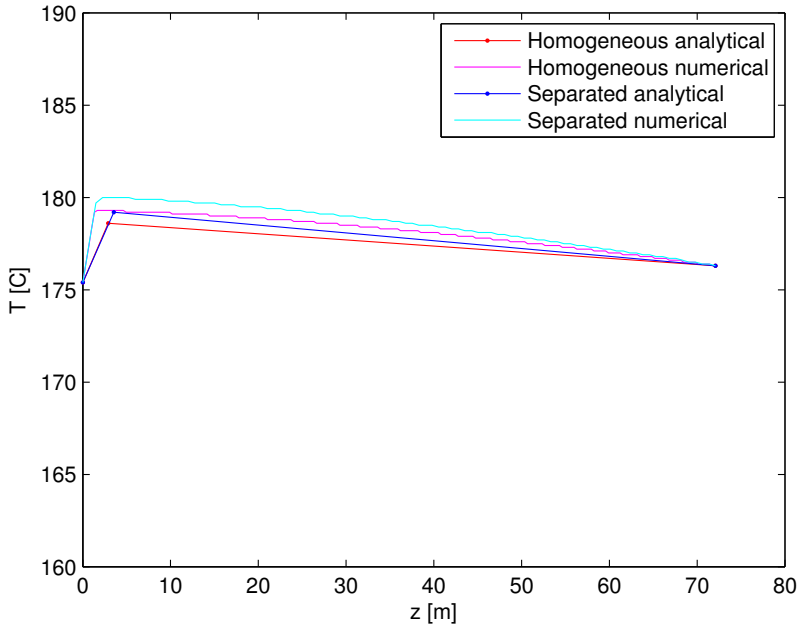

Figure 4.12: Saturation temperature - Four models comparison

As it can be seen the linear analytical curves overlap each other as the numerical ones do. The only observed differences between the models is the shorter sub-cooled region and higher saturation temperature for the numerical than for the analytical models, although the inlet and outlet temperatures are the same for the four models.

It should be noted here that, although the inlet pressure for each model is different, the inlet temperature is that of the drum for all the models, because the pump is assumed to be adiabatic and the liquid is not saturated at the inlet, the change in pressure does not affect its temperature.

4.8 Flow pattern determination

As introduced in section 1.5 the information obtained from the models can be used to determine the flow patterns that occur in the boiler. Two different flow maps for horizontal flow have been used together with the numerical separated flow model: the Baker flow map and the Taitel and Dukler flow map. It should be noted here that the influence of the turbulence the bends cause is not taken into account, but it is a fair assumption to ignore them, as the diamater of the tubes is much smaller than their length.

4.8.1 Baker flow map

This flow map uses two different parameters which work as coordinates to determine the flow pattern for the different flow conditions; on the horizontal axis $G_f\,\psi$ and G_g/λ on the vertical, with G_f and G_g the superficial mass velocities of the liquid and vapour phase respectively[1]. The λ and ψ factors are defined below [5]:

$$\psi = \left(\frac{\sigma_W}{\sigma}\right)\left[\left(\frac{\mu_l}{\mu_W}\right)\left(\frac{\rho_W}{\rho_l}\right)^2\right]^{1/3} \tag{4.2}$$

and

$$\lambda = \left[\left(\frac{\rho_g}{\rho_A}\right)\left(\frac{\rho_l}{\rho_W}\right)\right]^{1/2} \tag{4.3}$$

where the subscripts A and W refer to the values of the physical properties for air and water respectively at atmospheric pressure and temperature [5].

Figure 4.13 shows the calculated data points on the left and these drawn on the map on the right. According to these results, the transition from plug to slug flow happens around 3 meters in and the transition from slug to annular flow happens approximately 16.5 meters in. The flow is annular for the rest of the length of the pipe.

[1] This notation is only used here, for the sake of consistency with the Baker map formulation

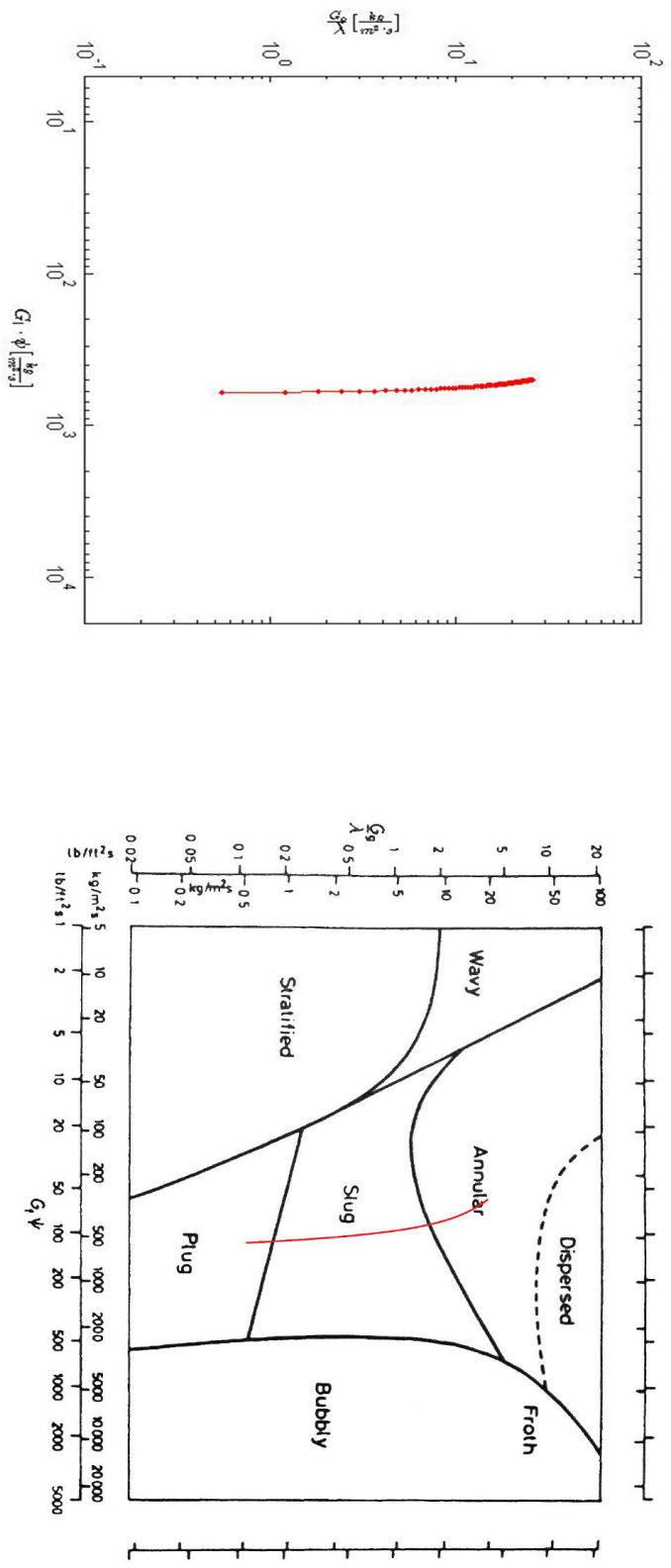

Figure 4.13: Baker flow map (The flow evolves from plug to annular) [5]

4.8.2 Taitel and Dukler flow map

The Taitel and Dukler flow map uses the Froude number Fr and the Martinelli parameter X to determine the flow pattern.

$$Fr = \frac{G_g}{[\rho_g(\rho_l - \rho_g)d\,g]^{1/2}} \tag{4.4}$$

and X is the square root of the quotient of the frictional pressure gradient if the liquid in the two-phase flow were flowing alone in the pipe and the frictional pressure gradient if the gas were flowing alone in the pipe [**?**]:

$$X = \left[\frac{(dp/dz)_l}{(dp/dz)_g}\right]^{1/2} \tag{4.5}$$

According to the Taitel and Dukler flow map, the flow starts as intermittent (plug/slug) flow and changes to annular around 16.5 meters in the pipe.

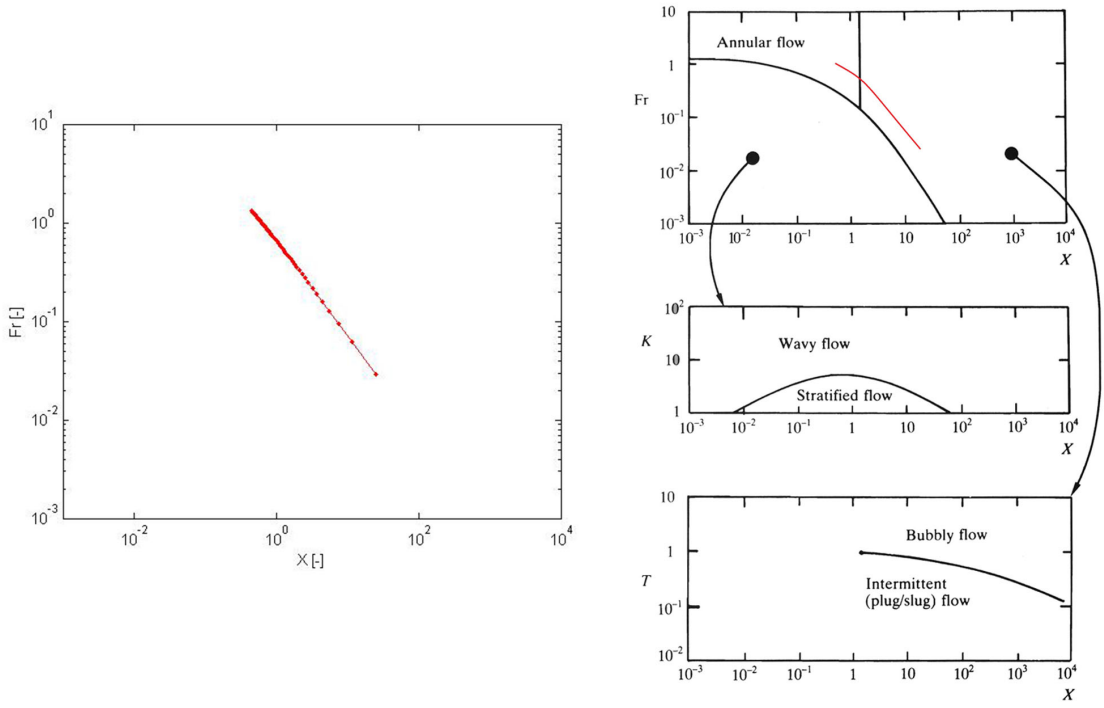

Figure 4.14: Taitel and Dukler flow map (The flow evolves from intermittent to annular) [4]

4.9 On the industry calculation method

As introduced in section 1.6 it is a common practice in industry to evaluate the effects of the pressure loss due to the presence of two-phase flow by considering a compensation horizontal saturation temperature profile. For the original design of the boiler described in chapter 2 a pressure loss of 0.5 bar was estimated with a very simple homogenous flow model. Being the pressure in the drum of 9 bar a mean pressure of 9.25 bar, was estimated and thus, the horizontal saturation temperature line used for the calculation of the heat transfer was set at the saturation temperature at that pressure [6]. The use of the numerical separated flow model shows that this method is perfectly valid for this particular study case: a horizontal temperature that results in the same amount of heat transfered is calculated, showing that it is only half a degree lower than the one estimated for the original design. Figures 4.15 and 4.16.

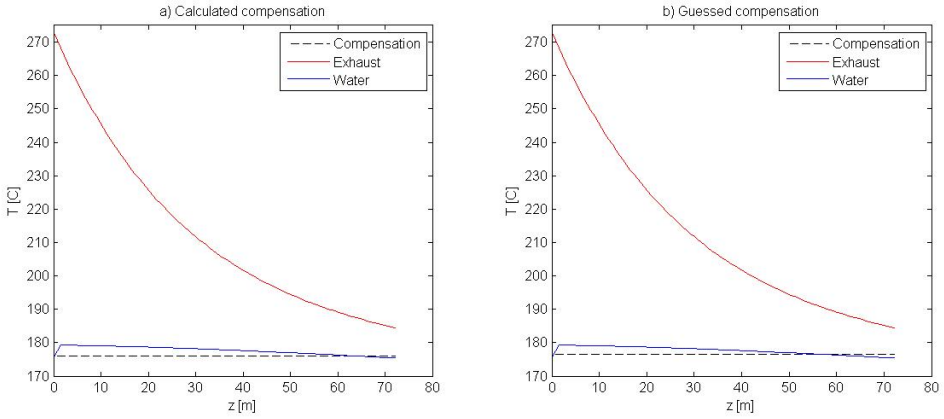

Figure 4.15: Temperature compensation method

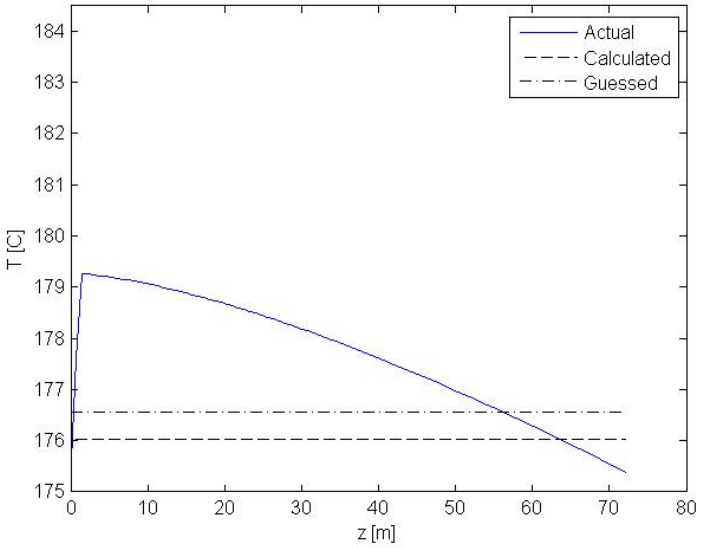

Figure 4.16: Temperature compensation method: zoom

5. Assessment studies

5.1 Introduction

There are different parameters that, for a given boiler, can be varied in the WHR installation. For instance, when a boiler for a marine WHR application is designed, its placement in the ship and where the drum will be is not always known in advance [6].

The drum pressure, while being an usual design parameter, might vary during operation, due to very high or very low steam demands, or might be found to be different to the specified design value. The analysis of lower installation pressures is also interesting as more pressure levels are expected to be introduced in the near future and boilers will be working under pressures as low as 3 or even 2 bar [12].

The water mass flow through the boiler is given by the intersection of the system characteristic curve with the pump curve. Although, as explained in the previous chapter, no pump curves are implemented in any of the calculations in this paper and the mass flow is considered to be fixed, it is interesting to study the effect of varying the mass flow in order to determine the characteristic curve of the system.

Parametric searches on these three independent variables are presented in this chapter, looking at how they affect the total pressure loss through the boiler and, therefore, the heat transfer, the outlet quality and the exhaust gas outlet temperature.

In addition to this, a study on the critical heat flux is offered at the end of the chapter.

As in the previous chapter all the studies are made under the same operating conditions, being the studied parameter the only one that is varied. The numerical separated flow model is the one used throughout all the chapter, since it is the one that gives most accurate results.

For the convenience of the reader these operating conditions are reproduced here again:

Exhaust gas mass flow	71.389	kg/s
Exhaust gas inlet temperature	273	°C
Exhaust gas pressure	104325	Pa
Water mass flow (to be studied as a parameter)	19.5	kg/s
Drum pressure (to be studied as a parameter)	9	bar
Return pipe pressure loss (to be studied as a parameter)	0.2	bar

Table 5.1: Operating conditions

5.2 Drum and boiler relative position: return pipe pressure loss

As shown in Figure 2.4 the drum is placed in level with the bottom of the boiler and as specified in Table 5.1 the return pressure loss from the outlet of the boiler to the steam drum is assumed to be of 0.2 bar. Return pressure loss can be easily related to the position of the drum, as for a pipe with given roughness and diameter, for a single phase flow, the pressure loss is a linear function of the length of the pipe (Equations 3.22, 3.23, 3.24 and 3.25). For two-phase flow this relation is no longer linear and relating the pressure loss to the pipe length is not a straightforward task. For this reason the studied parameter is the return pressure loss and not of the drum position, but the considered range of pressures, from 0 to 3 bar, with 0.1 bar steps, covers any possible location of the drum in the installation. At the same time, in a real scenario, if the drum was to be placed somewhere else than the design point, the diamater of the pipe would be changed accordingly so it produced the desired pressure loss, regardless of its length.

Figure 5.1 shows the total pressure loss through the boiler as a function of the return pressure loss. It can be seen that higher return pressure losses i.e. longer pipes between the boiler and the drum, result in lower pressure losses in an almost perfectly linear way.

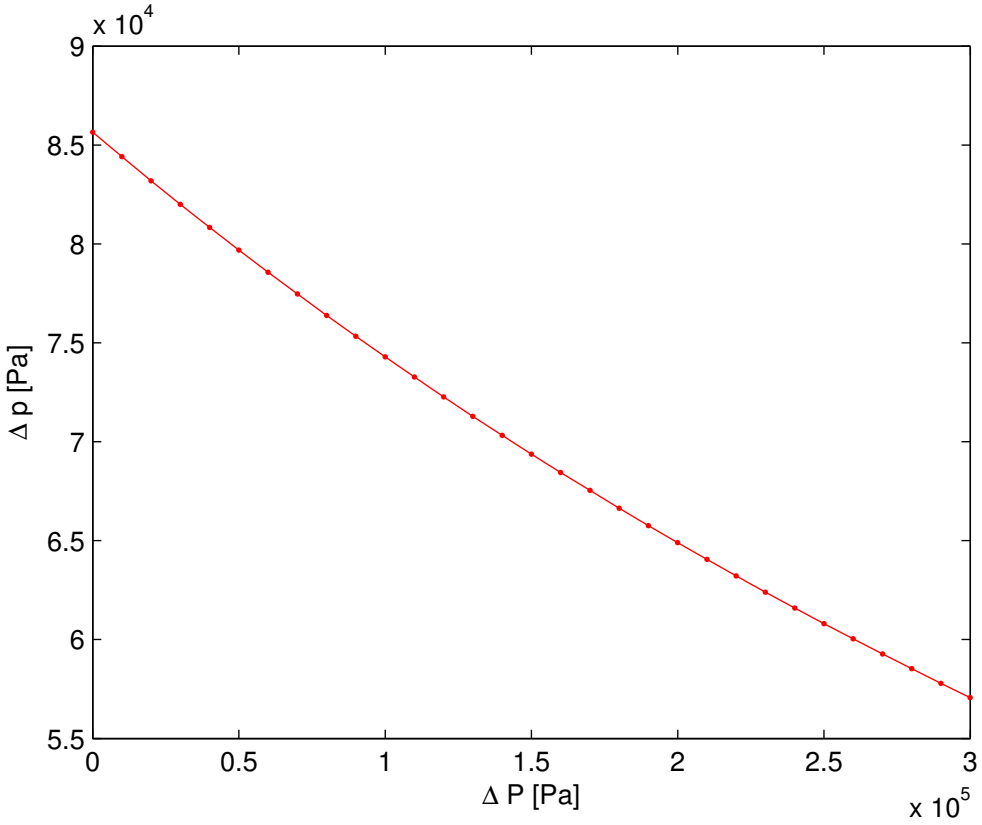

Figure 5.1: Pressure loss as a function of the return pressure loss

For a return pressure loss of 0 bar, corresponding to the case in which the boiler is directly and ideally connected to the drum with no pipe in between, the pressure loss through the

boiler is of 0.86 bar. The return pressure loss of the design point (0.2 bar) results in a pressure loss of 0.83 bar through the boiler. A return pressure loss of 3 bar, which would correspond to the maximum possible distance between drum and boiler (35 m), gives a pressure loss of 0.58 bar through the boiler.

This tendency is the expected one since, with a given drum pressure, higher pressure losses in the return pipe imply a higher pressure at the inlet of the boiler, making evaporation start later, having a shorter length of pipe in which two-phase flow occurs and, therefore, having a smaller pressure loss.

Figure 5.2 illustrates the linear relation between the length of the sub-cooled section and the return pipe pressure loss. For a return pressure loss of 0 bar the sub-cooled section is 1 m long, for the design point (0.2 bar return pipe pressure loss) it is 1.25 m long and 5 m for a return pressure loss of 3 bar.

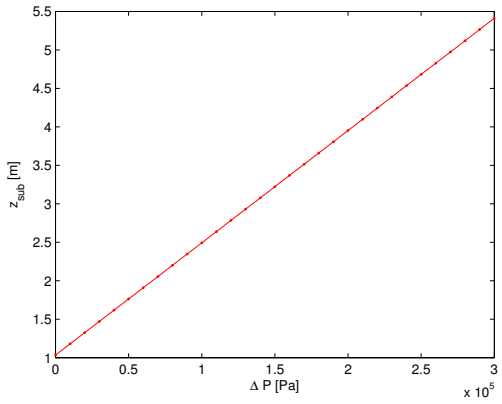

Figure 5.2: Sub-cooled length as a function of the return pressure loss

Figure 5.3 shows the total heat transfer, the outlet quality and the outlet temperatures, both for the water and the exhaust gas, as a function of the return pressure loss.

It can be observed that all these variables depend linearly on the return pressure loss: higher losses result in lower heat transfer, as they imply longer sub-cooled sections and less evaporation. It is interesting to observe that the outlet water temperature increases slightly faster than the exhaust gas outlet temperature, therefore decreasing the pinch point temperature difference. Table 5.2 summarizes the results for no return pressure loss, the design point and a return pressure loss of 1, 2 and 3 bar:

Return loss [bar]	ΔP [bar]	Q [MW]	x_o	T_{exh_o} [°C]	T_{w_o} [°C]	Pinch point [K]
0	0.86	6.667	0.168	184.5	175.4	9.1
0.2	0.83	6.607	0.165	185.3	176.3	9.0
1	0.74	6.377	0.152	188.4	179.9	8.5
2	0.66	6.117	0.138	191.9	184.1	7.8
3	0.58	5.854	0.123	195.4	188.0	7.4

Table 5.2: Return pressure loss parametric search results

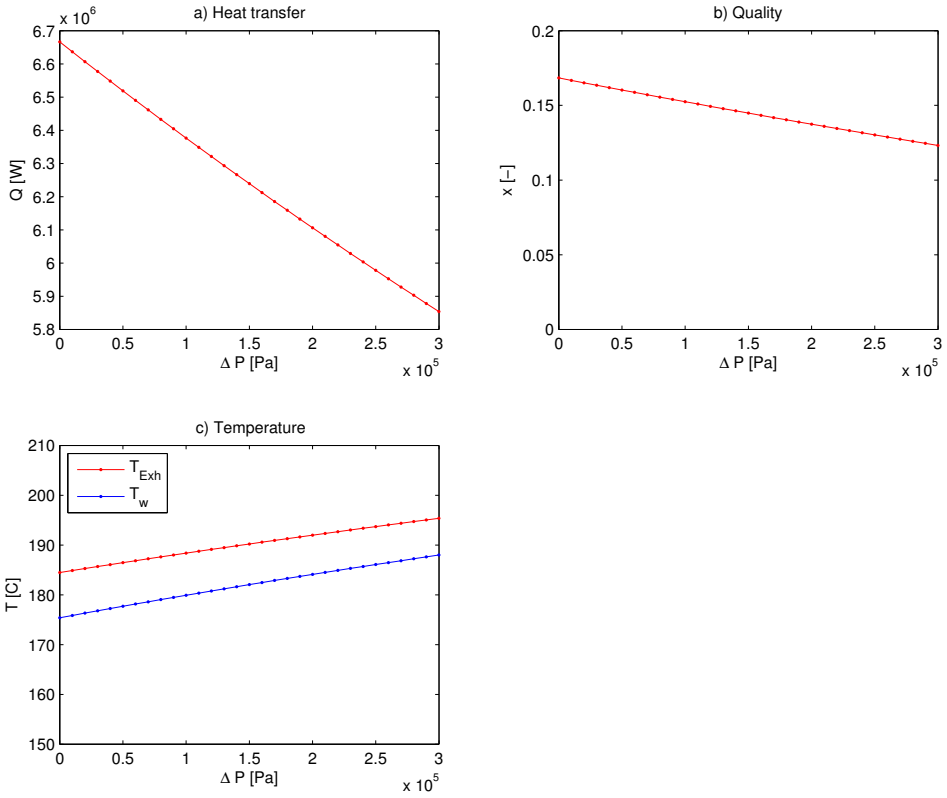

Figure 5.3: Heat transfer, quality and temperatures as a function of the return pressure loss

It can be easily concluded that a low as possible return pipe pressure loss is desired, as it considerably affects the amount of heat transfered, accounting for approximately 0.25 MW (4%) less transfered for each bar added to the return pressure loss.

5.3 Drum pressure

The parametric search on the drum pressure has been made for a range of pressures from 1.5 to 18 bar taking 0.5 bar steps.

Figure 5.4 shows the pressure loss through the boiler as a function of the drum pressure. As it can be seen, the lower the drum pressure the higher the pressure loss and vice versa, being more dependent on it at low pressure levels than at high ones. This is a logical result, since a lower drum pressure (lower pressure at the inlet as well) implies a lower saturation temperature and therefore a shorter sub-cooled length, as discussed in the previous section. The longer the evaporation section the higher the pressure loss is, but at the same time, the higher the heat transfered is as well. This can be seen in Figure 5.5, which shows the total heat transfer as a function of the drum pressure.

Figure 5.6 shows the dependencies of the quality and the exhaust gas and water outlet temperatures with the drum pressure. Following the same logic, higher drum pressures

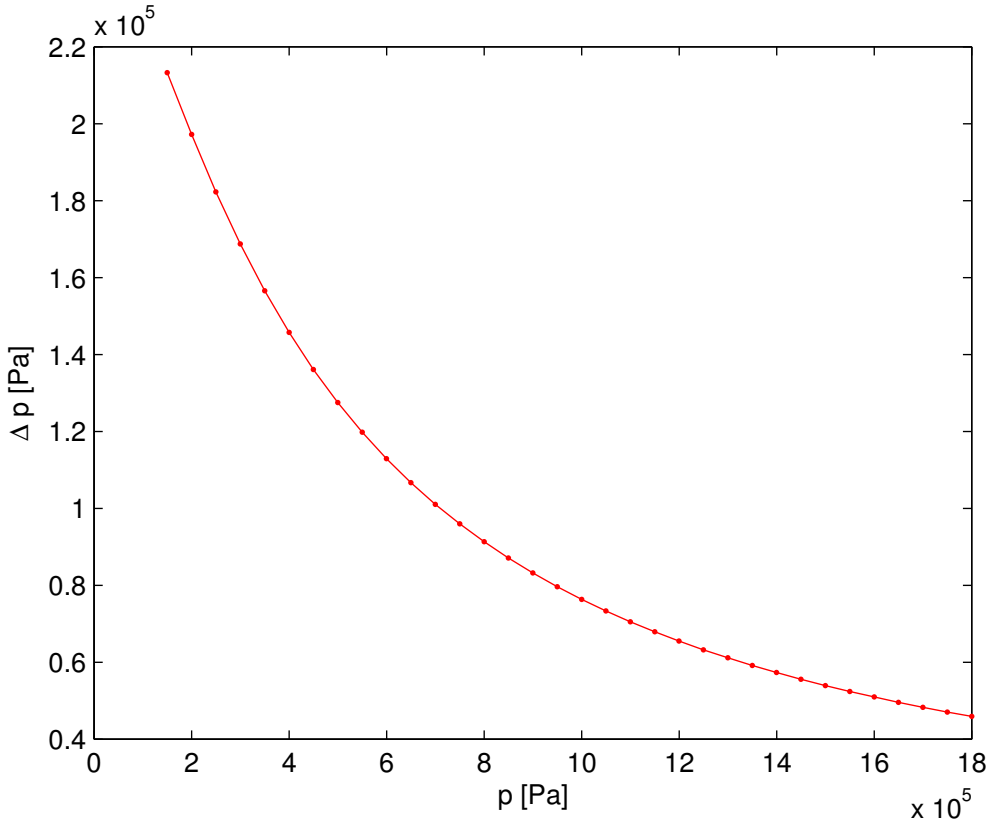

Figure 5.4: Pressure loss as a function of the drum pressure

account for less heat transfered, and therefore, less evaporation and less cooling of the exhaust gas. As the drum pressure and the outlet pressure of the boiler are linked, with a difference of 0.2 bar, it follows that the higher the drum pressure, the higher the saturation temperature at the outlet of the boiler. It should be noted that the two temperature curves tend to converge the higher the drum pressure gets, this meaning that the pinch point gets lower with high drum pressures, which is in accordance with the observed lower amount of heat transfered.

Results of this parametric search are summarized in Table 5.3, for drum pressures of 1.5, 4, 9 (design pressure), 15 and 18 bar.

Drum pressure [bar]	ΔP [bar]	Q [MW]	x_o	T_{exh_o} [°C]	T_{w_o} [°C]	Pinch point [K]
1.5	2.13	9.954	0.223	140.2	115.2	25.0
4	1.46	8.505	0.201	159.8	145.4	14.4
9	0.83	6.607	0.165	185.3	176.3	9.0
15	0.54	5.101	0.133	205.4	199.0	6.4
18	0.46	4.508	0.120	213.3	207.7	5.6

Table 5.3: Drum pressure parametric search results

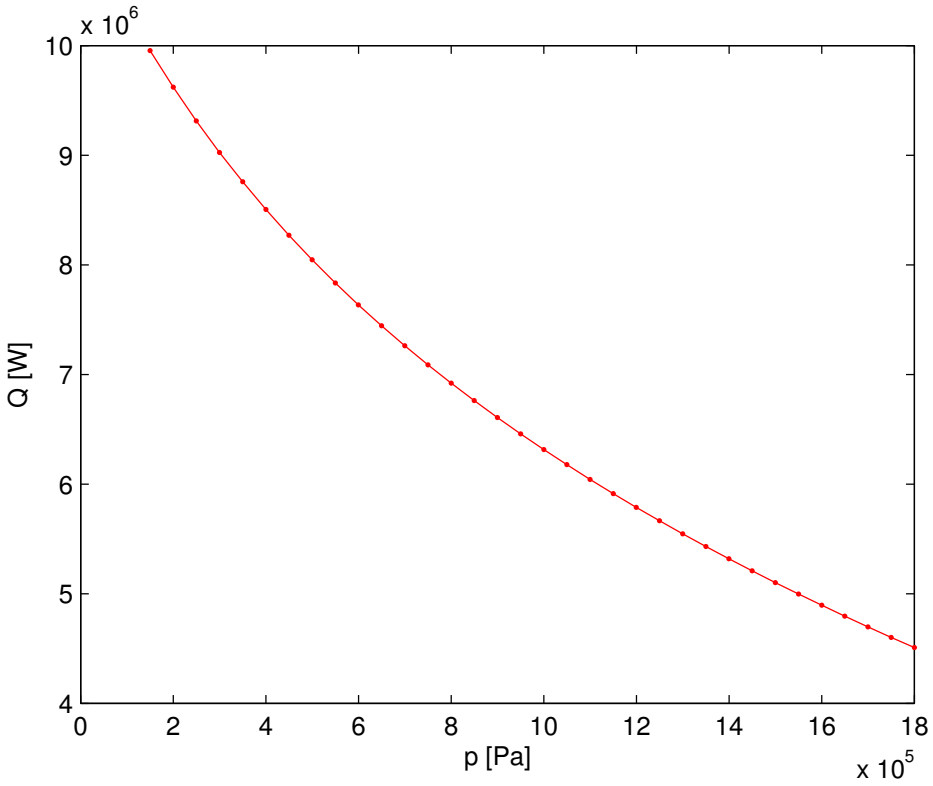

Figure 5.5: Total heat transfer as a function of the drum pressure

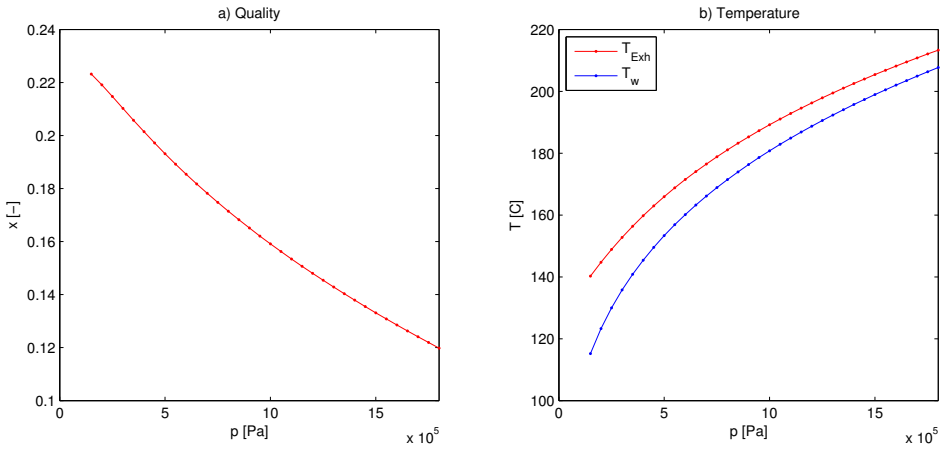

Figure 5.6: Quality and temperatures as a function of the drum pressure

It can be concluded that for a given boiler, that is, with a given heating surface area, lower drum pressures favor the heat transmission and this influence is stronger the lower the pressure of the system. In the pressure region below 9 bar a decrease in pressure of 1 bar (11%) results in approximately 0.5 MW (8%) more of heat transfered; in the pressure region above 9 bar, an increase in pressure of 1 bar (11%) results in 0.2 MW(3.2%) less heat transfered.

5.4 Mass flow: characteristic curve of the system

The characteristic curve of the system is determined running the model to determine the total pressure loss with different water mass flows through the boiler. Mass flows from 3.5 to 300 kg/s have been tested, producing the curve shown in Figure 5.7.

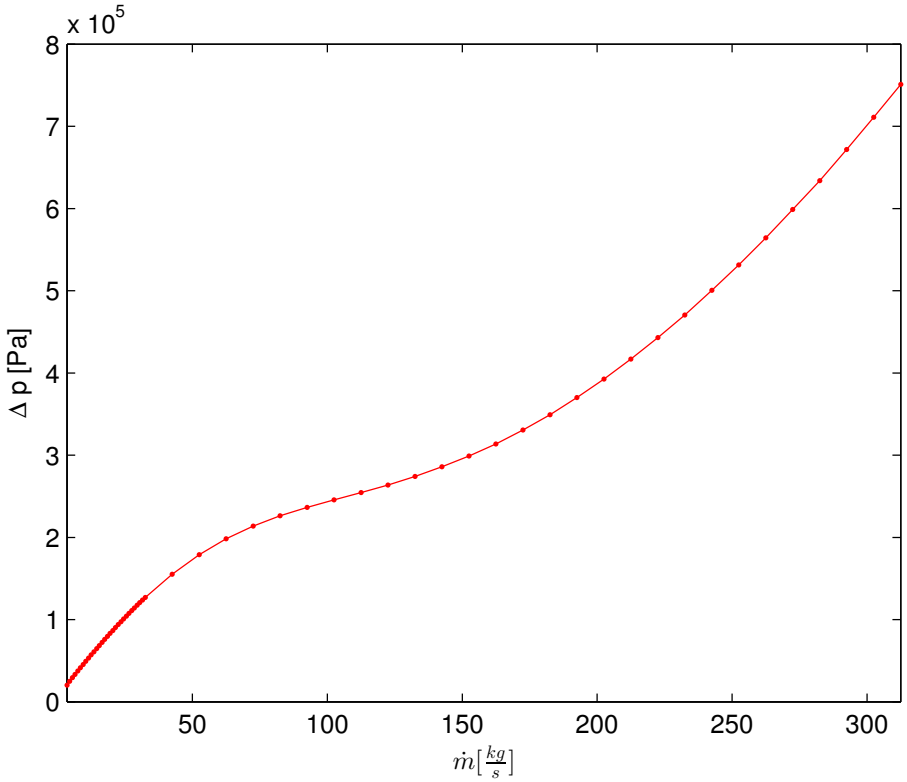

Figure 5.7: Pressure loss as a function of the water mass flow

The characteristic curve is used in conjunction with the pump curve to determine the working point of the system. Figure 5.8 shows a generic pump curve (to the left) on top of the system curve to illustrate how the mass flow through the system is determined by their intersection: the mass flow through the boiler is that which results in a pressure loss equal to the pressure increase the pump provides for that flow. On the right a pump curve that corresponds to the design mass flow of 19.5 kg/s is shown. A few comments on the Ledinegg instability are given in the next subsection.

As in the two previous parametric searches, the effect varying the mass flow has in the total heat transfer, the outlet quality and exhaust gas and water outlet temperatures has been studied too. Figure 5.9 shows the dependency of these three variables with the mass flow.

The heat transfer decreases linearly with the mass flow to a point where it reaches a minimum, for a mass flow of 125 kg/s and increases linearly, but with a less steep slope, for higher mass flows. The tendency for mass flows in the vicinity of the working region (19.5 kg/s) is easily explained by looking at the quality plot. For a given exhaust gas flow, a higher circulation (water mass flow) results in lower output qualities; as it can be seen

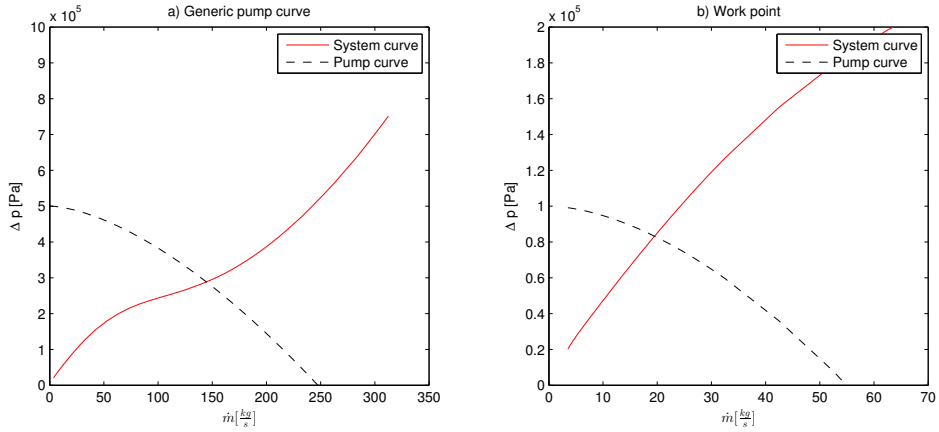

Figure 5.8: Pump curves and characteristic curve of the system

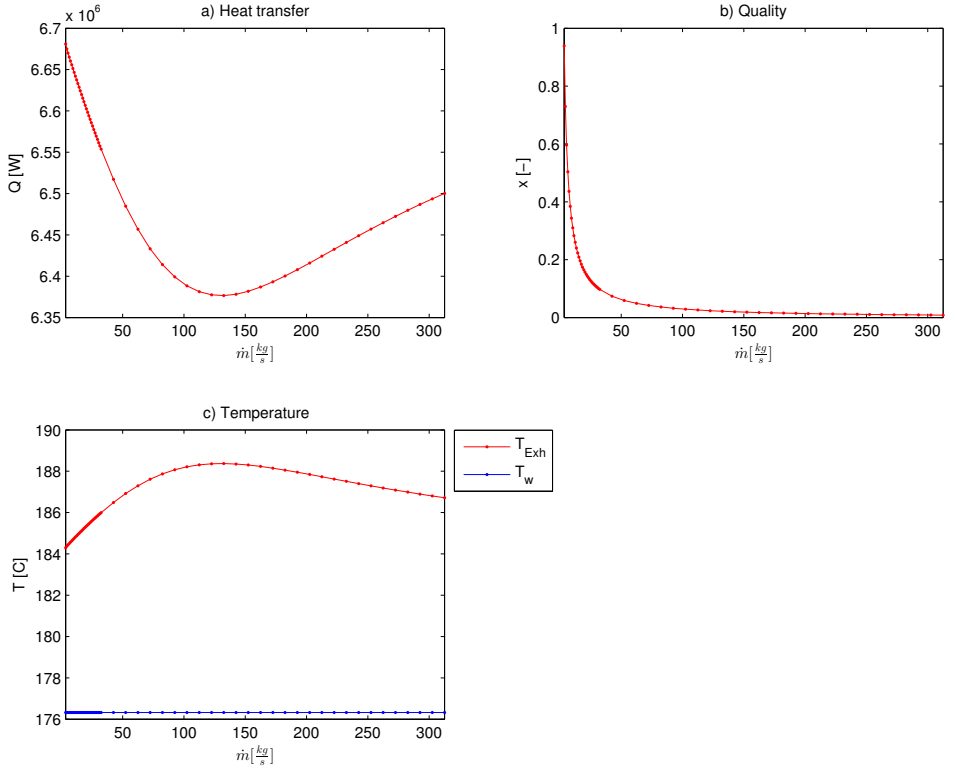

Figure 5.9: Heat transfer, qualities and temperatures as a function of the mass flow

in the quality graph, it decreases exponentially with the mass flow and, even though there is more water circulating, the amount of steam produced is lower. The difference in heat transfer between a mass flow of 3.5 kg/s and 125 kg/s is approximately 0.25 MW.

It is a curious phenomenon that the heat transfer reaches a minimum for a mass flow of 125 kg/s, and starts increasing with the mass flow from that point on. This can be explained again looking at the quality graph, which shows that for mass flows of 50 kg/s

or above the fraction of steam in the two-phase flow remains more or less stable at, roughly, 0.02. In this region, with a practically constant quality, a larger amount of water results in a larger amount of steam and, therefore, a higher heat transfer. It should be noted here that throughtout all this parametric search the return pipe pressure loss has been kept constant at a value of 0.2 bar, which is not a very realistic assumption, as the pressure loss is a function of the squared mass flow. This assumption makes the outlet pressure of the boiler to be kept constant at 9.2 bar and the outlet temperature at 176.3 °C, whereas a proper calculation of the return pressure loss would probably produce very different results. In any case, the region of interest is that around the design point of 19.5 kg/s, where the made assumptions are reasonable; results far beyond this point should be trated with great caution, as these assumptions are no longer valid.

Tendencies observed in the exhaust gas and water outlet temperatures can be explained in the same manner, and should, as well, be treated with caution for higher than 50 kg/s, as the model is out of its design region and results are not reliable.

Table 5.4 provides a summary of the results obtained from the parametric search.

Mass flow [kg/s]	ΔP [bar]	Q [MW]	x_o	T_{exh_o} [°C]	T_{w_o} [°C]	Pinch point [K]
3.5	0.20	6.681	0.939	184.3	176.3	8.0
19.5	0.83	6.607	0.165	185.3	176.3	9.0
52.5	1.79	6.485	0.059	186.9	176.3	10.3
122.5	2.64	6.377	0.024	188.4	176.3	12.1
202.5	3.93	6.416	0.014	187.8	176.3	11.5
300	7.11	6.494	0.009	186.8	176.3	10.5

Table 5.4: Mass flow parametric search results

It can be concluded that lower mass flows favor the heat transmission, as more evaporation is produced. At the same time, it can be concluded that the model should not be used to predict results for mass flows far from the design point, as some refinements should be implemented in order to represent reality in a more accurate way.

5.4.1 On the Ledinegg instability

The Ledinegg instability is a known two-phase flow static instability which occurs in heated pipes like the one modeled in this report [4].

Figure 5.10 shows a typical characteristic curve of a system like the one sketched. The shape of that curve is due to the pressure drop being proportional to the liquid density for low mass flows and to the gas density for high mass flows. As evaporation occurs, the pressure loss can decrease with higher mass flows because the gravitational pressure loss is decreasing relatively faster than the frictional pressure loss is increasing [4].

This is an undesired situation, since it provides three different working points for the same pump curve, and the system might be found to be working in an unstable one (y in the figure) where small changes in the mass flow would cause a big change in the pressure drop, forcing the system to move to one of the other two working points (x or z). In a

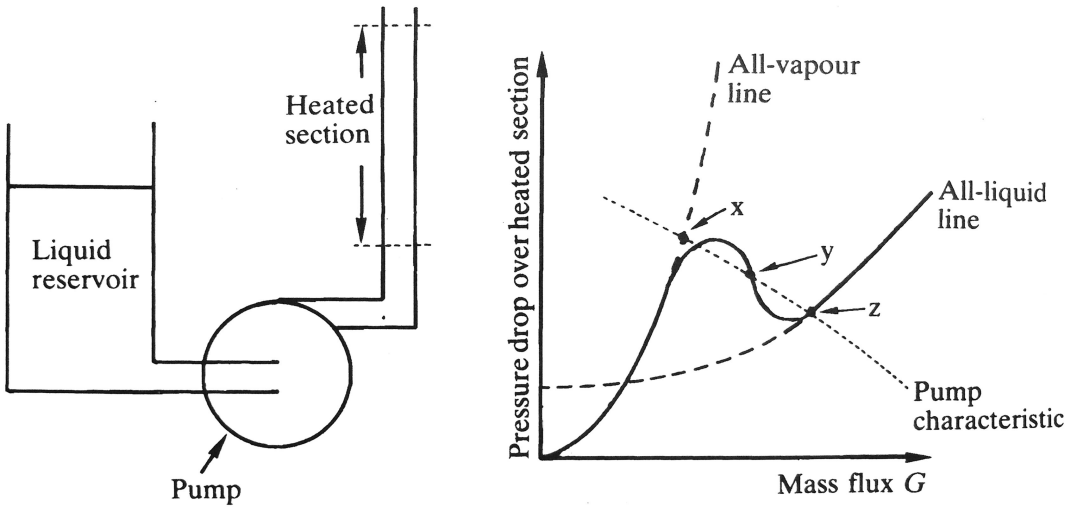

Figure 5.10: Heated pipe system and Ledinegg instability [4]

large boiler it could occur that some tubes work in point x, with a possible too small flow and too high quality that might result in exceding the critical heat flux (see next section); and others in z with a possible too small quality that would impoverish the heat transfer. [4]

Figure 5.11 shows the characteristic curve of the system and those of saturated water and saturated steam flowing through the boiler without any heat addition. It can be seen that the characteristic curve tends to converge with the saturated one for flows under 150 kg/s but starts separating from it afterwards. This odd tendency for mass flows above 150 kg/s can be explained in the same manner as for the heat transfer and quality results in this section: it is not sure that the separated flow model works well in regions so distant from the design point. In order to show the usual tendency, the analytical homogeneous flow model is used to produce the characteristic curve which, as it can be seen in the graph, tends to converge with that of the saturated water. In any case, it can be seen that the Ledinegg instability is not present in this system and, therefore, any chosen pump curve which cuts the system curve somewhere in the vicinity of the design point will work well. This result was expected, as studies show that the Ledinegg instability only occurs for high sub-cooling, defined as the difference between the inlet water temperature and the saturation temperature at the point where evaporation starts. In this system the sub-cooling is of 4.6 K; Ledinegg instability is not expected to occur for sub-cooling below 25 K [13].

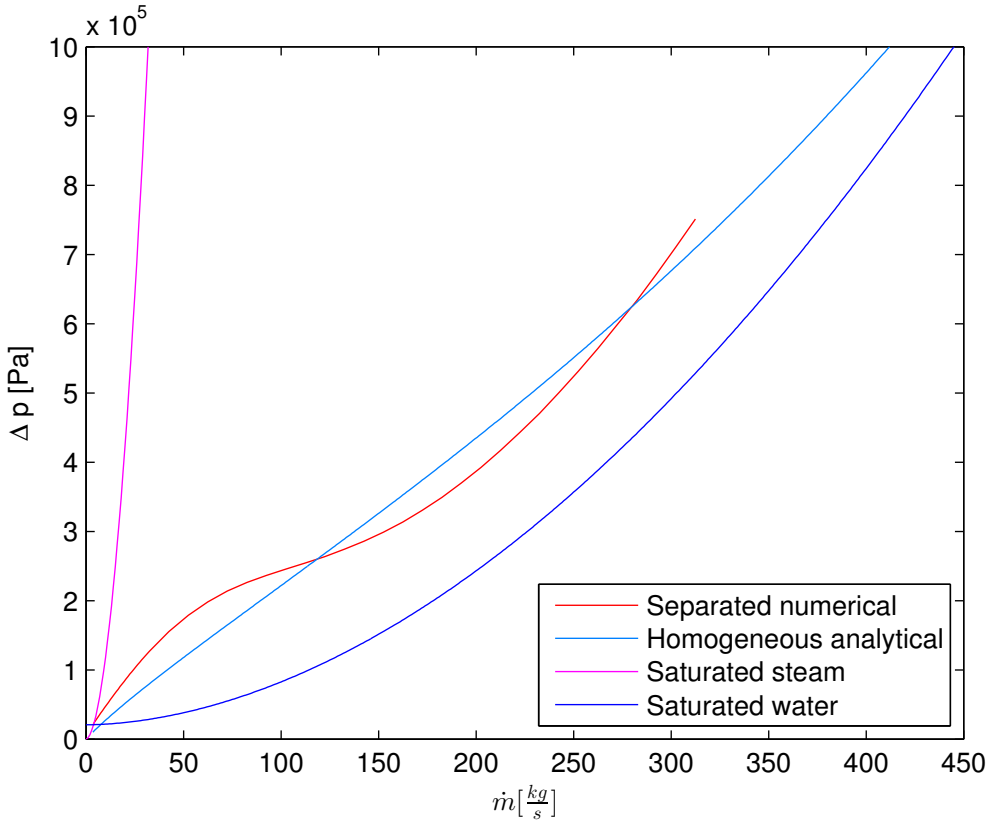

Figure 5.11: Characteristic curve with the separated flow and homogeneous flow models and saturated steam and water curves.

5.5 Critical heat flux

Critical heat flux or boiling crisis is reached when the heat flux from a surface to a fluid is so high that the liquid is separated from the heating surface by a layer of vapour. The heat transfer changes from a contact and liquid convection heat transfer to a radiation and gas convection heat transfer thereby increasing the temperature difference between the heating surface and the saturated liquid. It is necessary to make sure the critical heat flux is never reached as it may cause localised overheating in the pipe walls, being even possible to burn them [14].

Figure 5.12 shows the Nukiyama experiment results, which illustrates how heat fluxes beyond the critical point result in a sudden increase in the temperature difference between the wall and the liquid. Although this curve was obtained under very specific conditions, for a heated wire and pool boling, the concept of critical heat flux is the same and, anyway, correlations obtained for other configurations and boiling regimes are based on Nukiyama's conclussions and empirical derivations. [8]

For a horizontal pipe, the critical heat flux can be calculated by calculating the critical heat flux for a vertical pipe and applying the horizontal correction factor.

Tong and Tang developed a correlation based on experimental data by Celata and Mariani for the critical heat flux in a vertical pipe [15]:

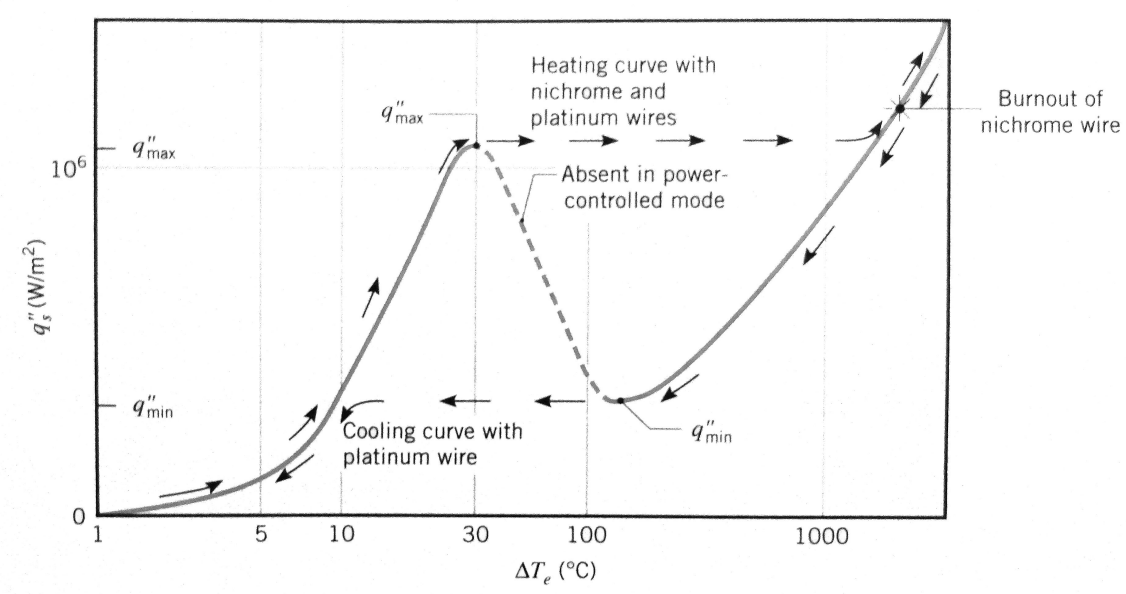

Figure 5.12: Nukiyama's experiment: critical heat flux [8]

$$\ddot{Q}_{crit} = \frac{C_1\, h_{fg}\, \rho_l\, U_o}{Re^{0.6}} \tag{5.1}$$

where h_{fg} is the water latent heat, the Reynolds number is defined as

$$Re = \frac{\rho_l\, U_o\, d}{\mu_{sat}} \tag{5.2}$$

and

$$U_o = \frac{G}{\rho_h} \tag{5.3}$$

$$C_1 = (0.216 + 4.74\, 10^{-}2\, p)\, \psi \tag{5.4}$$

$$\psi = \frac{1}{2 + 30\, x_o} \tag{5.5}$$

Then the critical heat flux for a horizontal pipe is given by:

$$\ddot{Q}_{crit,hor} = \ddot{Q}_{crit,vert}\, K \tag{5.6}$$

A good correction factor K is [15]:

$$K = 1 - e^{-(\frac{T_1}{3})^{0.5}} \tag{5.7}$$

with

$$T_1 = C_1\, Re_l^{-0.2}\, (\frac{1-x}{1-\alpha})\, (\frac{G^2}{g\, d_{in}\, \rho_l\, (\rho_l - \rho_g)\, \alpha^{0.5}}) \tag{5.8}$$

Figure 5.13 shows the critical heat flux along the length of the pipe and the heat flux obtained from the model. As it can be seen the critical heat flux is of the order of eight times higher than the heat flux for every point of the pipe and, therefore, it can be concluded that the boiler is operating without the risk of burnout due to this phenomenon.

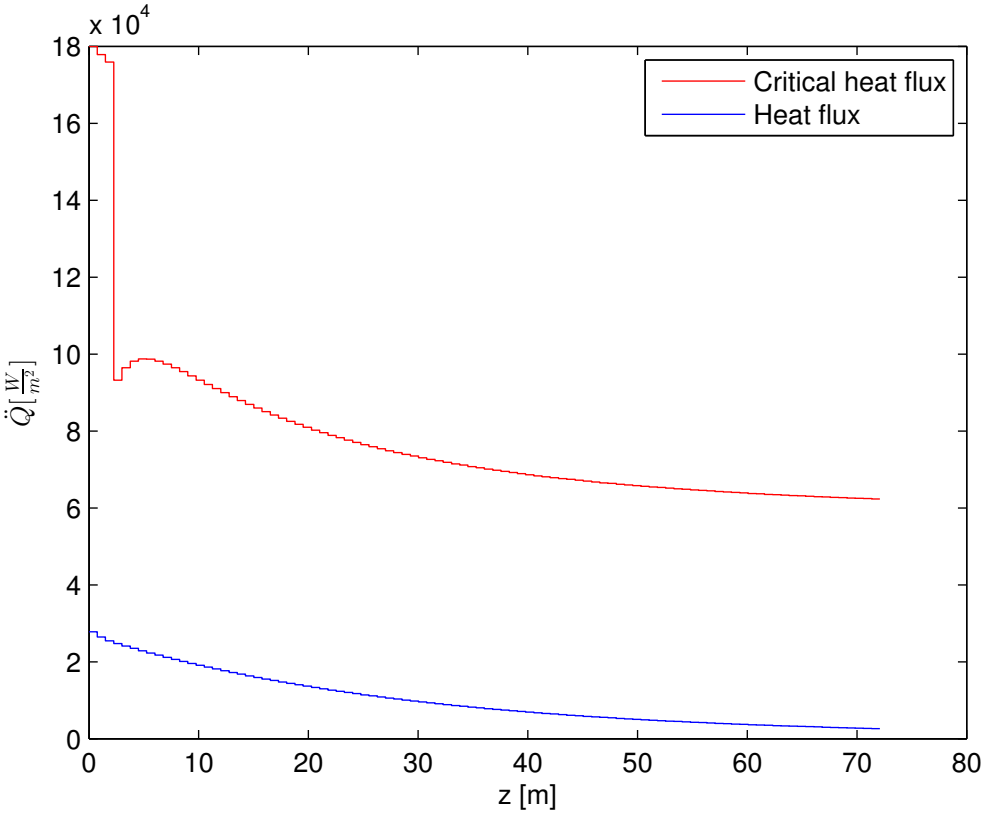

Figure 5.13: Critical heat flux

6. Conclusions

6.1 Introduction

Conclusions from the analysis carried out in this paper can be drawn in two directions, first the adequacy of using analytical or numerical homogeneous or separated flow models for two-phase flow boiler calculations and, second, the effects of chosing one system configuration or another for a given boiler design.

6.2 On the models

6.2.1 Homogeneous flow vs. separated flow models

It is concluded from the obtained results that it is preferable to build and use a separated flow model than a homogeneous flow one to study the effects of two-phase flow in marine WHR boilers. The evaluation of the pressure loss with the separated flow model gives a more realistic result, with the obtention of pressure losses up to a 60% higher than those obtained with the more optimistic homogeneous flow model, although results for the total heat transfer differ in only about 2%.

If the total heat transfer is the only variable of interest, boiler designers might want to use homogeneous flow models, since the difference in the results between those and the separated flow ones are minimal and the first are easier to develop.

6.2.2 Analytical vs. numerical models

It is obvious that if a pressure, temperature, quality or heat flow profile is required, the use of numerical models is mandatory, as the analytical ones only calculate inlet and outlet properties and assume a linear evolution between those. For the same reason it is as well advisable to build and use numerical models for the calculation of the total pressure loss, as these show drops about 25% higher than the analytical ones. In regard to the total heat transfer results show that the use of numerical models predict more conservative results, being the difference of around 2%. Also, numerical models are the only ones that can be used for the determination of flow patterns.

As observed above, if the only variable of interest is the total heat transfer, boiler designers might want to use analytical models, since they are much easier to develop and the results they give for this parameter are within the same accuracy as those given by the numerical models.

Taking these discussions into account, it can be said that whenever the knowledge of temperature, quality or heat flow needs to be known for a specific point or the flow pattern needs to be determined, a separated flow numerical model is the best choice.

When predicting the total heat transfer is the main goal, it is perfectly possible to do so with the simplest model, the analytical homogeneous flow one, which gives results as precise as those obtained with the most complex model.

In general, since taking effect of the pressure drop into account mainly affects the temperature in the first meters of pipe, the overall heat transfer calculation is not greatly improved by introducing complex two-phase flow considerations.

6.3 On the system configuration and operating conditions

The conclusiond drawn from the assessment studies in the previous chapter are summarized here:

- For the given boiler design it is desirable to have the lowest possible return pipe pressure loss. Increments of 1 bar in the return pressure loss result in around 0.25 MW less of heat transfered (3.75%).

- For the given boiler design, lower system pressures are desired, as in the normal marine WHR region of working pressures, a decrease of 1 bar in the drum pressure results in 0.5 MW more of heat transfered (7.6%).

- For the given boiler design, the system is observed to be stable and lower mass flows favour the heat transmission.

- It is concluded as well, that for the region of possible working conditions, there is no risk of reaching the critical heat flux in any point of the boiler.

7. Future work

With a longer time limit several things in this project could be improved and extended. Being the drawn conclussions valid as they are to serve as recommendations for future marine WHR boiler design projects, their reliability could be enhanced with the following improvements in the work:

- Modelling of the whole system, taking all the pipe dimensions of the installation into account.
- Introduction of a real pump curve, which would represent how real systems work, without a fixed mass flow through the boiler, unlike the system described in this paper.
- Use of a better software, in order to have higher resolution in the numerical models, which would allow to observe the development of the flow better.
- Implementation of flow pattern models, utilizing the existing equations for this analysis approach in order to obtain a more precise pressure profile.
- Contrast the results with measurements from a real system, which would allow to validate the results and assess the reliability of the models.
- Development of dynamic models, which would allow to study the system under time-variating conditions, such as sudden increases in the steam demand.

A. Influence of the bends in the friction factor

This appendix offers a detailed calculation of the extra component added to the friction factor in order to compensate for the influence of the bends, which are eliminated in the model:

$$\Delta p = f \cdot \frac{1}{2} \cdot \frac{L}{d} \cdot \frac{G^2}{\rho} + n_{bends} \cdot \zeta \cdot \frac{1}{2} \cdot \frac{G^2}{\rho} \tag{A.1}$$

$$\Delta p = f_{fric+bend} \cdot \frac{1}{2} \cdot \frac{L}{d} \cdot \frac{G^2}{\rho} \tag{A.2}$$

$$f_{fric+bend} \cdot \frac{1}{2} \cdot \frac{L}{d} \cdot \frac{G^2}{\rho} = f \cdot \frac{1}{2} \cdot \frac{L}{d} \cdot \frac{G^2}{\rho} + n_{bends} \cdot \zeta \cdot \frac{1}{2} \cdot \frac{G^2}{\rho} \tag{A.3}$$

$$f_{fric+bend} \cdot \frac{L}{d} \cdot \frac{G^2}{\rho} = f \cdot \frac{L}{d} \cdot \frac{G^2}{\rho} + n_{bends} \cdot \zeta \cdot \frac{G^2}{\rho} \tag{A.4}$$

$$f_{fric+bend} \cdot \frac{L}{d} = f \cdot \frac{L}{d} + n_{bends} \cdot \zeta \tag{A.5}$$

$$f_{fric+bend} = f + n_{bends} \cdot \zeta \cdot \frac{d}{L} \tag{A.6}$$

$$\zeta = 1 \tag{A.7}$$

$$n_{bends} = 18 \tag{A.8}$$

$$d = 0.03[m] \tag{A.9}$$

$$L = 72.09[m] \tag{A.10}$$

$$n_{bends} \cdot \zeta \cdot \frac{d}{L} = 18 \cdot 1 \cdot \frac{0.03}{72.09} = 0.0749 \tag{A.11}$$

$$f \approx 0.01 \div 0.02 \tag{A.12}$$

$$f_{fric+bend} \approx 0.01749 \div 0.02749 \tag{A.13}$$

B. CEA NASA Data

Figure B.1 provides the density, specific enthalpy and specific heat capacity at different temperatures. These properties, for temperatures between and including 0 and 1000 °C are used to generate functions for the properties for any given temperature in that range.

Heavy Fuel Exhaust Gas Properties $\lambda = 3$ No Dissociation

Temp °C	ρ kg/m^3	h kJ/kg	c_p kJ/kg K	u kJ/kg	C_v kJ/kg K	MW kg/kmol
0.00	1.2985	0.0000	1.0160	0.0000	0.7303	29.1041
25.00	1.1896	25.4346	1.0188	18.2925	0.7332	29.1041
50.00	1.0976	50.9438	1.0220	36.6597	0.7363	29.1041
75.00	1.0187	76.5350	1.0254	55.1088	0.7397	29.1041
100.00	0.9505	102.2164	1.0292	73.6481	0.7435	29.1041
125.00	0.8908	127.9969	1.0333	92.2867	0.7477	29.1041
150.00	0.8382	153.8862	1.0379	111.0338	0.7522	29.1041
175.00	0.7914	179.8931	1.0428	129.8987	0.7571	29.1041
200.00	0.7496	206.0265	1.0480	148.8901	0.7623	29.1041
250.00	0.6780	258.7050	1.0593	187.2845	0.7737	29.1041
300.00	0.6188	311.9772	1.0717	226.2725	0.7860	29.1041
350.00	0.5692	365.8834	1.0847	265.8946	0.7990	29.1041
400.00	0.5269	420.4482	1.0980	306.1753	0.8123	29.1041
450.00	0.4905	475.6810	1.1113	347.1240	0.8256	29.1041
500.00	0.4587	531.5780	1.1245	388.7369	0.8388	29.1041
550.00	0.4309	588.1244	1.1373	430.9992	0.8516	29.1041
600.00	0.4062	645.2977	1.1496	473.8884	0.8639	29.1041
650.00	0.3842	703.0708	1.1613	517.3774	0.8756	29.1041
700.00	0.3645	761.4159	1.1724	561.4384	0.8868	29.1041
750.00	0.3467	820.3074	1.1831	606.0458	0.8974	29.1041
800.00	0.3305	879.7173	1.1932	651.1715	0.9075	29.1041
850.00	0.3158	939.6134	1.2026	696.7836	0.9169	29.1041
900.00	0.3023	999.9654	1.2114	742.8514	0.9257	29.1041
950.00	0.2900	1060.7449	1.2197	789.3468	0.9340	29.1041
1000.00	0.2786	1121.9254	1.2275	836.2432	0.9418	29.1041
1050.00	0.2681	1183.4827	1.2348	883.5164	0.9491	29.1041
1100.00	0.2583	1245.3940	1.2416	931.1437	0.9559	29.1041
1150.00	0.2492	1307.6389	1.2481	979.1044	0.9624	29.1041
1200.00	0.2408	1370.1978	1.2542	1027.3792	0.9685	29.1041
1250.00	0.2329	1433.0530	1.2600	1075.9503	0.9743	29.1041
1300.00	0.2255	1496.1882	1.2654	1124.8014	0.9797	29.1041
1350.00	0.2185	1559.5881	1.2705	1173.9171	0.9849	29.1041
1400.00	0.2120	1623.2385	1.2754	1223.2834	0.9897	29.1041
1450.00	0.2058	1687.1267	1.2801	1272.8875	0.9944	29.1041
1500.00	0.2000	1751.2404	1.2845	1322.7170	0.9988	29.1041
1550.00	0.1945	1815.5684	1.2886	1372.7610	1.0030	29.1041
1600.00	0.1893	1880.1003	1.2926	1423.0088	1.0069	29.1041
1650.00	0.1844	1944.8265	1.2964	1473.4509	1.0107	29.1041
1700.00	0.1798	2009.7380	1.3000	1524.0782	1.0143	29.1041
1750.00	0.1753	2074.8264	1.3035	1574.8824	1.0178	29.1041
1800.00	0.1711	2140.0837	1.3068	1625.8557	1.0211	29.1041
1850.00	0.1671	2205.5027	1.3100	1676.9906	1.0243	29.1041
1900.00	0.1632	2271.0767	1.3130	1728.2804	1.0273	29.1041
1950.00	0.1595	2336.7988	1.3159	1779.7186	1.0302	29.1041
2000.00	0.1560	2402.6638	1.3187	1831.2993	1.0330	29.1041
2050.00	0.1527	2468.6655	1.3214	1883.0170	1.0357	29.1041
2100.00	0.1495	2534.7988	1.3239	1934.8661	1.0383	29.1041
2150.00	0.1464	2601.0586	1.3264	1986.8419	1.0408	29.1041
2200.00	0.1434	2667.4404	1.3288	2038.9397	1.0431	29.1041
2250.00	0.1406	2733.9399	1.3311	2091.1550	1.0455	29.1041
2300.00	0.1378	2800.5530	1.3334	2143.4839	1.0477	29.1041
2350.00	0.1352	2867.2754	1.3355	2195.9224	1.0498	29.1041
2400.00	0.1327	2934.1038	1.3376	2248.4666	1.0519	29.1041
2450.00	0.1302	3001.0347	1.3396	2301.1133	1.0539	29.1041
2500.00	0.1279	3068.0647	1.3416	2353.8594	1.0559	29.1041
2550.00	0.1256	3135.1909	1.3435	2406.7012	1.0578	29.1041
2600.00	0.1234	3202.4102	1.3453	2459.6365	1.0596	29.1041
2650.00	0.1213	3269.7200	1.3471	2512.6621	1.0614	29.1041
2700.00	0.1193	3337.1174	1.3488	2565.7754	1.0631	29.1041
2750.00	0.1173	3404.6003	1.3505	2618.9741	1.0648	29.1041
2800.00	0.1154	3472.1660	1.3521	2672.2559	1.0664	29.1041
2850.00	0.1136	3539.8125	1.3537	2725.6182	1.0680	29.1041
2900.00	0.1118	3607.5376	1.3553	2779.0591	1.0696	29.1041
2950.00	0.1100	3675.3394	1.3568	2832.5767	1.0711	29.1041
3000.00	0.1084	3743.2158	1.3583	2886.1689	1.0726	29.1041

(1) **This table does NOT include dissociation** (Properties calculated by CEA-NASA (version 2003))
(2) Above table based on the (mass fraction) gas composition at 25°C and $1.01325 \cdot 10^5$ Pa
$O_2 = 0.15065$ $N_2 = 0.73752$ Ar $= 0.012612$ $CO_2 = 0.075305$ $H_2O = 2.9344 \cdot 10^{-2}$
$SO_2 = 7.534 \cdot 10^{-4}$ $\sum = 1.0000$
(3) Gas constant (at 25°C) $R = 285.68$ J/kmol K based on a $R_u = 8314.51$ J/kmol K
(4) Based on Heavy Fuel Oil (86.8% C 11% H 0.86% N 1.81% S)
Air humidity 30% at 25°C - 0.0094738 kmol water/kmol dry air (0.0059 kg water/kg dry air)

Figure B.1: Exhaust gas data from CEA NASA

C. Convergence study

Since it is not possible to use the maximum resolution in the numerical models for every calculation, as EES can only compute a limited amount of variables, a convergence study to analyze the influence of changes in resolution has been carried out. The results presented in Tables C.1 and C.2 show that the number (and size) of the elements in the models is not determinant, as can be observed in the calculated deviations for the total pressure drop and the total heat transfer for both numerical models:

Steps	Step size	ΔP [Pa]	Deviation [%]	Q [W]	Deviation [%]	$T_{exh_{out}}$ [°C]	x
219	0.32918	66421	0	6623764.9	0	185.0	0.165
144	0.50063	66420	0.00	6623964.6	0.00	185.0	0.165
96	0.75094	66421	0.00	6624251.7	0.01	185.0	0.165
72	1.00125	66418	0.01	6624573.0	0.01	185.0	0.165
54	1.335	66442	-0.03	6624887.7	0.02	185.0	0.165
48	1.50188	66411	0.02	6625123.8	0.02	185.0	0.165
36	2.0025	66355	0.1	6625898.5	0.03	185.0	0.165
24	3.00375	66306	0.17	6627474.8	0.06	185.0	0.165
18	4.005	66265	0.23	6629084.6	0.08	185.0	0.165
15	4.806	66220	0.3	6630396.1	0.10	185.0	0.165
12	6.0075	66120	0.45	6632399.9	0.13	185.0	0.165
9	8.01	65859	0.85	6635833.0	0.18	185.0	0.165
6	12.015	64992	2.15	6643007.3	0.29	184.9	0.166
4	18.0225	62927	5.26	6654384.3	0.46	184.9	0.166
3	24.03	60098	9.52	6666282.5	0.64	184.8	0.166
2	36.045	52649	20.74	6690827.5	1.01	184.7	0.167
1	72.09	21098	68.24	6760100.2	2.06	184.1	0.168

Table C.1: Convergence search: homogeneous flow model

Steps	Step size	ΔP [Pa]	Deviation [%]	Q [W]	Deviation [%]	$T_{exh_{out}}$ [°C]	x
96	0.75094	83193	0	6606814.6	0	185.2	0.165
72	1.00125	83174	0.02	6607127.5	0.00	185.2	0.165
54	1.335	83163	0.04	6607507.8	0.01	185.2	0.165
48	1.50188	83157	0.04	6607649.1	0.01	185.2	0.165
36	2.0025	83113	0.1	6608327.8	0.02	185.2	0.165
24	3.00375	83105	0.11	6609934.1	0.05	185.2	0.165
18	4.005	83131	0.07	6611575.5	0.07	185.2	0.165
15	4.806	83161	0.04	6612913.2	0.09	185.2	0.165
12	6.0075	83209	-0.02	6614959.8	0.12	185.2	0.165
9	8.01	83286	-0.11	6618472.7	0.18	185.2	0.165
6	12.015	83395	-0.24	6625851.7	0.29	185.2	0.165
4	18.0225	83393	-0.24	6637683.4	0.47	185.1	0.165
3	24.03	83167	0.03	6650255.9	0.66	185.0	0.166
2	36.045	82019	1.41	6676951.4	1.06	184.9	0.166
1	72.09	73310	11.88	6760099.6	2.32	184.1	0.168

Table C.2: Convergence search: separated flow model

D. On the choice of software: Engineering Equation Solver

The Engineering Equation Solver, EES, is the software chosen for the implementation of the computer model, as it contains thermodynamic properties libraries for the fluid considered in this paper (as well as for many others) and has many in-built heat transfer functions. Its capacity and way of simultaneously solving up to 6000 non-linear equations [16] makes it specially suitable for the purpose of this project, as these can be written in any order and it is EES itself who carries out the tedious iterative process inherent to heat exchanger calculations, as some variables need to be guessed for a first calculation and progressively corrected until results are found to converge.

Some additional features that make EES a convenient software are its capacity for unit conversion and automatic unit consistency checking, its feature for parametric studies and the possibility of graphic plotting.

The choice is also a matter of academic consistency, since EES is taught and used in many heat transfer courses in engineering faculties and student licenses are often provided by them[1].

[1]The software copy and license used for the elaboration of this paper have been provided by the Department of Energy Technology at Aalborg University

E. Convective boiling heat transfer coefficient

There are many ways of determining the heat transfer coefficient of a flowing and boiling liquid. In 1963 J. C. Chen compared a number of different correlations using a representative selection of experimental data points where by the Chen correlation was shown to be the most precise [5] In 1953 Rohsennow proposed the assumption of superposition of the nucleate and convective heat transfer coefficients [15]

$$h_{TP} = h_{NB} + h_c \tag{E.1}$$

Where h_{NB} is the nucleate boiling heat transfer coefficient and h_c is the convective heat transfer coefficient.
Chen built on that suggesting the use of a Dittus-Boelter type equation was to represent the convective heat transfer coefficient [5]

$$h_c = 0.023 \cdot Re_{TP}^{0.8} \cdot Pr_{TP}^{0.4} \cdot \frac{k_{TP}}{d} \tag{E.2}$$

Where it is normally assumed that the Reynolds number, Prandtl number and conductivity are calculated based on the liquid vapour mixture Chen argued that since most flows have contact between the pipe and the liquid phase they should be calculated for the liquid phase. Chen defined a parameter F so that [15]

$$F = (\frac{Re_{tp}}{Re_f})^{0.8} = (\frac{Re_{tp} \cdot \eta_f}{G \cdot (1-x) \cdot d})^{0.8} \tag{E.3}$$

whereby h_c becomes

$$h_c = 0.023 \cdot F \cdot (\frac{G \cdot (1-x) \cdot d}{\eta_f})^{0.8} \cdot (\frac{\eta \cdot c_p}{k})^{0.4} \cdot (\frac{k_f}{d}) \tag{E.4}$$

Forster and Zuber analysed pool boiling in 1955 and found that for pool boiling the mean superheat of the fluid in which the bubble grows is lower than the wall superheat and that the difference between the two superheats and thus neglected in pool boiling. In forced convection however they cannot be neglected [15]

$$h_{NB} = 0.00122 \cdot (\frac{k_l^{0.79} \cdot c_{pf}^{0.45} \cdot \rho_f^{0.49}}{\sigma^{0.5} \cdot \eta_f^{0.29} \cdot h_{fg}^{0.24} \cdot \rho_g^{0.24}}) \cdot \Delta T_o^{0.24} \cdot \Delta Po^{0.75} \tag{E.5}$$

Where ΔT_o is the mean superheat Chen defined a suppression factor S as the ratio between the mean superheat and the wall superheat [15]

$$S = (\frac{\Delta T_o}{\Delta T_{sat}}) = (\frac{\Delta T_o}{\Delta T_{sat}})^{0.24} \cdot (\frac{\Delta P_o}{\Delta p_{sat}})^{0.75}) \tag{E.6}$$

Where ΔT_o is the mean superheat and ΔT_{sat} is the wall superheat Thus creating

$$h_{NB} = 0.00122 \cdot S \cdot (\frac{k_l^{0.79} \cdot c_{pf}^{0.45} \cdot \rho_f^{0.49}}{\sigma^{0.5} \cdot \eta_f^{0.29} \cdot h_{fg}^{0.24} \cdot \rho_g^{0.24}}) \cdot \Delta T_{sat}^{0.24} \cdot \Delta P_{sat}^{0.75} \tag{E.7}$$

Bibliography

[1] Wenzhi G, Junmeng Z, Guanghua L, Qiang B, Liming F. Performance Evaluation and Experiment System for Waste Heat Recovery of Diesel Engine. Energy. 2013;(50):226–235.

[2] Hossain SN, Bari S. Waste Heat Recovery From the Exhaust of Diesel Generator Using Rankine Cycle. Energy Conversion and Manegement. 2013;(75):141–151.

[3] Waste heat Recovery System (WHRS), for Reduction of Fuel Consumption, Emissions and EEDI. MAN Diesel & Turbo; 2013.

[4] Whalley JB. Boiling, Condensation and Gas-Liquid Flow. 1st ed. Oxford University Press; 1987. ISBN: 978-0-19-856234-4.

[5] Collier JG, Thome JR. Convective Boiling and Condensation. 3rd ed. Oxford University Press; 1996. ISBN: 0-19-856296-9.

[6] Condra TJ. Associate Professor at the Department of Energy Enigneering, AAU; 2014.

[7] CEA-NASA. NASA; 2014. Available from: `http://www.grc.nasa.gov/WWW/CEAWeb/ceaHome.htm`.

[8] Incropera FP, Dewitt DP, Bergman TL, Lavine AS. Fundamentals of Heat and Mass Transfer. 6th ed. John Wiley and Sons; 2007. ISBN: 978-0-471-45728-2.

[9] Baker C, Vuppuluri P, Shi L, Hall M. Model of Heat Exchangers for Waste Heat Recovery From Diesel Engine Exhaust for Thermoelectric Power. Journal of Electronic Materials. 2012;41(6):1290–1297.

[10] Manickam M, Schwarz MP, Perry J. CFD Modeling of Waste Heat Recovery Boiler. Applied Mathematical Modelling. 1998;(22):823–840.

[11] et al RCA. Heat Exchanger Design Handbook, Fluid Mechanics and Heat Transfer. 1st ed. Hemisphere Publishing Corporation; 1986. ISBN: 0-89116-125-2.

[12] Sorensen K. Associate Professor at the Department of Energy Enigneering, AAU; 2014.

[13] Bertelsen TB, Larsen M. Investigation of instabilities in concentrated solar power plants. 2012;.

[14] Kefer V, Köhler W, Kastner W. Critical Heat Flux (CHF) and Post-CHF Heat Transfer In Horizontal and Inclined Evaporator Tubes. International Journal of Multiphase Flow. 1988;15(3):385–392.

[15] Tong LS, Tong YS. Boiling Heat Transfer and Two-Phase Flow. 2nd ed. Taylor and Francis; 1997. ISBN: 1-56032-485-6.

[16] EES. http://www.fchart.com/ees/;.